Nonlinear magnetoelectric metamaterials: Analysis and homogenization via a microscopic coupled-mode theory

Alec Rose, Stéphane Larouche, Ekaterina Poutrina, and David R. Smith
Center for Metamaterials and Integrated Plasmonics, Duke University, Durham, North Carolina 27708, USA
(Received 10 August 2012; published 12 September 2012)

Artificially structured metamaterials hybridized with elements that respond nonlinearly to incident electromagnetic fields can, from a macroscopic perspective, support nonlinear responses that cannot be described by purely electric or magnetic interactions. To investigate the mechanisms and behaviors of such interactions, termed nonlinear magnetoelectric coupling, we develop a set of coupled-mode equations for describing three-wave mixing in a metamaterial, using Bloch modes as the basis. By equating these coupled-mode equations to those of a homogenized system, we derive closed-form expressions for the macroscopic nonlinear susceptibilities. From these expressions, a great deal can be inferred about the nature and construction of magnetoelectric nonlinearities in metamaterials. As an example, we apply this method in the analysis of a prototypical nonlinear magnetoelectric metamaterial. In particular, we show that independent control of the eight second-order susceptibility tensors encompasses a massive parameter space from which new realms of nonlinear interference and wave manipulation can be accessed.

DOI: 10.1103/PhysRevA.86.033816 PACS number(s): 42.70.Nq, 42.65.Ky, 75.85.+t, 81.05.Xj

I. INTRODUCTION

The manipulation of electromagnetic radiation is an immense field at the heart of much of modern technology, relying on a wide array of light-matter interactions. In particular, certain materials respond to electromagnetic waves in such a way that the incident electric and magnetic fields are coupled through the medium itself. In other words, the medium is electrically polarized by both incident electric *and* magnetic fields, and likewise can be magnetically polarized by both electric and magnetic fields. These materials are variously known as bianisotropic, chiral, magnetoelectric, and optically active, depending on the context and classification, but they all involve some interdependence of the electric and magnetic responses and fields. The recent surge of research into artificial mediums composed of periodic, subwavelength, polarizable elements has in turn sparked interest in these magnetoelectric interactions (for a review of the subject, see Refs. [1–3] and references within). Even though these artificial media, known collectively as metamaterials (MMs), are typically composed of dielectric and metal components, their geometry can be tailored to support circulating currents—the essence of magnetic response [4]. Through careful design of the metamaterial elements, the incident electric and magnetic fields can be coupled to the medium and each other through supported intraelement modes, as in dipolar resonances, and interelement modes, as in magnetoinductive coupling [5,6]. MMs can thus access strong and tailorable electric, magnetic, and magnetoelectric responses [7,8], and even mimic the magnetic phenomena of natural materials [9–11]. Chiral metamaterials have received particular attention for applications requiring a distinction between left and right circularly polarized light [12–19]. Through manipulation of these electric, magnetic, and magnetoelectric responses, MMs have been used to demonstrate a variety of novel and anomalous properties, including negative refraction [12,20] and electromagnetic cloaking [21,22].

It is very likely, however, that the greatest potential for unique electromagnetic media lies in the particular subclass of MMs hybridized with nonlinear components—components whose electromagnetic responses display relatively strong nonlinear dependencies on the incident fields. Through careful design, these nonlinear MMs are capable of combining drastically reduced nonlinear length scales with the exotic and configurable wave propagation that is characteristic of MMs. Numerous studies have revealed the advantages of such materials, promising greatly enhanced nonlinear interactions [4,23–27], exotic parametric configurations [28–32], and interesting soliton dynamics [33–36], to name a few. Indeed, the parameter space for nonlinear MMs is virtually boundless, often probing effects and phenomena that are conventionally neglected.

An interesting subset of this parameter space lies in the overlap between nonlinear and magnetoelectric responses, that is, nonlinear interactions that involve coupling between *both* electric and magnetic field components. To give context to this subset of light-matter interactions, it is useful to consider the usual form for the macroscopic polarization and magnetization vectors. Following the convention of nonlinear optics, the material response is expanded in a power series [37], in which the higher-order contributions are taken to be proportional to the product of two or more incident fields. Thus, we can write the first-order (linear) polarization and magnetization vectors as

$$\vec{P}(t) = \sum_n \left[\epsilon_0 \bar{\bar{\chi}}^{(1)}_{ee}(\omega_n)\vec{E}(\omega_n) + \frac{i}{c}\bar{\bar{\chi}}^{(1)}_{em}(\omega_n)\vec{H}(\omega_n) \right] e^{-i\omega_n t}, \tag{1}$$

$$\mu_0\vec{M}(t) = \sum_n \left[\mu_0 \bar{\bar{\chi}}^{(1)}_{mm}(\omega_n)\vec{H}(\omega_n) + \frac{i}{c}\bar{\bar{\chi}}^{(1)}_{me}(\omega_n)\vec{E}(\omega_n) \right] e^{-i\omega_n t}, \tag{2}$$

respectively, where ϵ_0 and μ_0 are the permittivity and permeability of free space, c is the speed of light in free space, the summation is taken over all positive and negative frequencies ω_n, and $\bar{\bar{\chi}}^{(1)}$ are the rank-2 linear susceptibility tensors. Analogous to Eqs. (1) and (2), one can envision higher-order polarizations that are proportional to both the electric *and* magnetic fields, or even a combination thereof,

constituting what we shall refer to as nonlinear magnetoelectric coupling. In a three-wave mixing process, the addition of magnetoelectric terms leads to a fourfold increase in the number of independent nonlinear susceptibilities, as given by the following definitions of the second-order polarization:

$$\begin{aligned}\vec{P}^{(2)}(t) = \sum_{qr} \big[& \bar{\bar{\chi}}^{(2)}_{eee}(\omega_s;\omega_q,\omega_r) : \vec{E}(\omega_q)\vec{E}(\omega_r) \\ & + \bar{\bar{\chi}}^{(2)}_{emm}(\omega_s;\omega_q,\omega_r) : \vec{H}(\omega_q)\vec{H}(\omega_r) \\ & + \bar{\bar{\chi}}^{(2)}_{eem}(\omega_s;\omega_q,\omega_r) : \vec{E}(\omega_q)\vec{H}(\omega_r) \\ & + \bar{\bar{\chi}}^{(2)}_{eme}(\omega_s;\omega_q,\omega_r) : \vec{H}(\omega_q)\vec{E}(\omega_r)\big] e^{-i\omega_s t}, \end{aligned} \quad (3)$$

and second-order magnetization:

$$\begin{aligned}\mu_0\vec{M}^{(2)}(t) = \sum_{qr} \big[& \bar{\bar{\chi}}^{(2)}_{mmm}(\omega_s;\omega_q,\omega_r) : \vec{H}(\omega_q)\vec{H}(\omega_r) \\ & + \bar{\bar{\chi}}^{(2)}_{mee}(\omega_s;\omega_q,\omega_r) : \vec{E}(\omega_q)\vec{E}(\omega_r) \\ & + \bar{\bar{\chi}}^{(2)}_{mme}(\omega_s;\omega_q,\omega_r) : \vec{H}(\omega_q)\vec{E}(\omega_r) \\ & + \bar{\bar{\chi}}^{(2)}_{mem}(\omega_s;\omega_q,\omega_r) : \vec{E}(\omega_q)\vec{H}(\omega_r)\big] e^{-i\omega_s t}, \end{aligned} \quad (4)$$

where $\sum_{qr}$ denotes a double sum over all positive and negative frequencies, ':' implies a tensor inner product between the rank-3 second-order susceptibility tensors and the field vectors, and $\omega_s = \omega_q + \omega_r$. For higher-order processes, the number of possible susceptibility tensors grows exponentially. While nonlinear magnetoelectric responses are known to exist in natural materials [38–43], their applications are largely limited to material studies [44–46]. Most device-oriented applications of second-order nonlinear optics, such as wave-mixing and parametric processes, utilize just $\chi^{(2)}_{eee}$-type nonlinearities [37], stemming from the fact that, at optical frequencies, the magnetic responses of natural materials tend to be exceedingly weak.

In this paper, we show that MMs are not only able to support the full set of nonlinear responses, including the magnetoelectric terms, but can do so simultaneously and in a variety of combinations, while retaining or even *enhancing* the superior strengths of $\chi^{(2)}_{eee}$-type materials. Extrapolating from the recent research in linear MMs, it is likely that a wealth of phenomena not previously available will follow from tailoring the eight nonlinear susceptibilities in Eqs. (3) and (4), as well as their higher-order counterparts. To deal with such a staggering increase in the available nonlinear properties and subsequent dynamics, a coherent description of the magnetoelectric nonlinearities, their effects, and their origins is necessary. Towards this end, we investigate the relation between the subwavelength geometry of the MM inclusions, and the homogenized, constitutive properties of the bulk nonlinear MM itself.

For a lossless medium composed of a cubic lattice of MM inclusions formed from electrically polarizable materials, we make use of a coupled-mode theory formalism to derive simple, quasianalytic expressions for the eight effective magnetoelectric nonlinearities. For example, the effective second-order susceptibility relating an electric polarization at frequency ω_3 to the product of an electric field at ω_1 and a magnetic field at ω_2 is shown to be

$$\chi^{(2)}_{eem}(\omega_3;\omega_1,\omega_2) = \frac{i}{a^3}\iiint \big[\bar{\bar{\chi}}^{(2)}_{loc}(\vec{r}) : \vec{\theta}_1(\vec{r})\vec{\phi}_2(\vec{r})\cdot\vec{\theta}_3(\vec{r})\big] dV, \quad (5)$$

where $\bar{\bar{\chi}}^{(2)}_{loc}(\vec{r})$ is the MM's local electric nonlinear susceptibility tensor and a is the lattice constant. $\vec{\theta}_n(\vec{r})$ and $\vec{\phi}_n(\vec{r})$ are, roughly speaking, the *microscopic* electric fields produced in response to a *macroscopic* electric or magnetic field, respectively, at frequency ω_n, and can be found analytically and/or numerically from a Bloch analysis of a particular MM geometry. These expressions for the second-order susceptibilities are verified against existing nonlinear parameter retrieval methods [47,48], finding excellent agreement. We extend the same procedure to the case of four-wave mixing in MMs, finding analogous relations for the 16 effective third-order magnetoelectric nonlinearities. Further study of these expressions gives insight into the fundamental nature and construction of the various magnetoelectric nonlinearities. In particular, the formalism is demonstrated in the analysis of two prototypical nonlinear magnetoelectric MMs, predicting the dominant nonlinearities and wave-mixing processes supported in each, in agreement with recent experiments [49]. Finally, we give some consideration to possible applications of nonlinear magnetoelectric coupling, using the examples of nonlinear interference and electro-optic-like effects.

II. DERIVATION OF THE EFFECTIVE NONLINEAR SUSCEPTIBILITIES

Our purpose in this section is to derive a homogeneous description of three-wave mixing in a nonlinear MM with a periodic microstructure of electrically polarizable materials. In other words, we seek the set of effective nonlinear properties that can exactly reproduce the MM's macroscopic nonlinear behavior. Conceptually, we correlate the nonlinear scattering observed or computed for a MM to what would be obtained from a homogeneous medium with defined linear and nonlinear constitutive parameters. This approach to MM effective-medium theory has been used with great success to characterize linear MMs [50–56]; for example, a popular MM retrieval procedure involves computing the scattered (reflected and transmitted) waves from a thin slab of MM, and inverting the Fresnel formulas to ascribe homogenized values of the electric permittivity and magnetic permeability to the otherwise inhomogeneous medium [51]. The approach works extremely well to describe MMs formed with inclusions of nearly any shape or material composition, under a restricted set of assumptions. Alternatively, one can appeal to the basic nature of effective-medium theory and apply averages over the computed microscopic fields associated with a given repeated MM cell to arrive at the homogenized, macroscopic fields. From these macroscopic fields, the effective constitutive parameters can be derived. Both methods have been shown to be in agreement with each other and with conventional effective-medium approaches [52]. Regardless of the method, the final set of effective properties not only simplifies the subsequent analysis of MMs, but provides invaluable intuition into their design.

While a nonlinear medium can be exceedingly complex, coupling potentially an infinite set of harmonics or mix components with varying polarization and propagation directions, it is typically the case that the nonlinear response—even for most MMs—is relatively small compared with the linear response. Thus, the nonlinearity can be treated as a perturbation, coupling together a restricted number of fundamental and harmonic or mix waves. Under this assumption of a perturbative nonlinear response, only a small subset of scattered waves needs to be considered, making the problem far more tractable. For a homogeneous nonlinear medium under continuous-wave excitation, coupled-wave theory [57–59] yields relatively straightforward expressions for the spatially varying wave amplitudes in terms of the underlying parameters of the medium. When applied in integral form, coupled-mode theory can provide similar expressions for an inhomogeneous medium in terms of integrals over the local variations. In this way, coupled-mode theory offers an approach—in the same spirit as field averaging—for the identification of effective nonlinear susceptibility parameters in a MM comprising periodically positioned inclusions of arbitrary shape and composition. Thus, the specific goals of this section are threefold: first, to present coupled-wave theory in the present context; second, to derive the coupled-mode expressions for a MM in terms of its microscopic structure; and last, to equate these expressions with those for a homogeneous medium described by (3) and (4), yielding a set of eight relations for the eight macroscopic second-order susceptibilities.

A. Coupled-wave equations for wave-mixing processes in a homogeneous medium

It is useful to first consider how waves couple in a homogeneous nonlinear medium, for which the nonlinearity—taken as an electric second-order susceptibility—is relatively weak. We imagine a three-wave mixing process involving three monochromatic waves. In the absence of the nonlinearity, the medium supports transverse electromagnetic (TEM) plane waves, for which we employ the wave label μ to denote frequency, polarization, and direction. Thus, each wave can be described by electric field

$$\vec{E}_\mu = A_\mu \vec{e}_\mu e^{i\vec{k}_\mu\cdot\vec{r}} \tag{6}$$

and magnetic field

$$\vec{H}_\mu = A_\mu \vec{h}_\mu e^{i\vec{k}_\mu\cdot\vec{r}}, \tag{7}$$

where A_μ is the wave amplitude, and $\vec{e}_\mu$ and $\vec{h}_\mu$ are the corresponding polarization vectors. We take the polarization vectors to be normalized such that

$$\tfrac{1}{2}(\vec{e}_\mu \times \vec{h}^*_\mu + \vec{e}^*_\mu \times \vec{h}_\mu) = \hat{s}_\mu, \tag{8}$$

where $\hat{s}_\mu$ is the unit normal in the direction of the Poynting vector. Due to the frequency decomposition convention used here, the wave intensity is given by $I_\mu = 2\mathrm{Re}(\vec{E}_\mu \times \vec{H}^*_\mu) = 2|A_\mu|^2$. Treating the nonlinearity as a perturbation, we can consider its effect on these traveling waves via the coupled-wave equation (A9), derived from Maxwell's equations in Appendix A. In this way, we can consider the effect of waves 1 and 2, with frequencies ω_1 and ω_2, respectively, on wave 3 at the sum frequency $\omega_3 = \omega_1 + \omega_2$, according to

$$\nabla\cdot[A_3(\vec{e}_3 \times \vec{h}^*_3 + \vec{e}^*_3 \times \vec{h}_3)] = i\omega_3[\vec{P}^{(2)}\cdot\vec{e}^*_3 + \vec{M}^{(2)}\cdot\vec{h}^*_3]e^{-i\vec{k}_3\cdot\vec{r}}. \tag{9}$$

Thus, the perturbation is seen to induce a spatial variance in the sum-frequency mode amplitude A_3. If we assume a purely electric nonlinearity, such that

$$\vec{P}^{(2)} = 2\bar{\bar{\chi}}^{(2)}_{eee} : \vec{E}_1\vec{E}_2 = 2A_1A_2\bar{\bar{\chi}}^{(2)}_{eee} : \vec{e}_1\vec{e}_2 e^{i(\vec{k}_1+\vec{k}_2)\cdot\vec{r}}, \tag{10}$$

and neglect $\vec{M}^{(2)}$, then the coupled-wave equation takes the familiar form [59]

$$\nabla A_3(\vec{r})\cdot\hat{s}_3 = i\omega_3 A_1(\vec{r})A_2(\vec{r})\bar{\bar{\chi}}^{(2)}_{eee} : \vec{e}_1\vec{e}_2\cdot\vec{e}^*_3 e^{i(\vec{k}_1+\vec{k}_2-\vec{k}_3)\cdot\vec{r}}. \tag{11}$$

The above equation makes apparent the various interdependencies of the wave amplitudes and momenta, and the medium nonlinearity. Furthermore, we could consider the nonlinear polarizations arising at the fundamental frequencies, resulting in two additional coupled-wave equations. Together with the proper initial conditions, these equations allow a full description of the evolution of the three waves.

If we now replace the continuous nonlinear medium with a MM, we expect to obtain an expression similar to that above, with coupling proportional to an effective or averaged nonlinear susceptibility, rather than the intrinsic susceptibility. In fact, given the various responses available in MM inclusions, Eq. (11) will in general include both a magnetic and an electric response, in addition to magnetoelectric terms. These other terms are usually not significant in conventional materials, but can be dominant in structured MMs. Continuing with the homogeneous perspective, the above coupled-wave analysis can be straightforwardly extended to consider the full contributions from Eqs. (3) and (4), yielding

$$\nabla A_3(\vec{r})\cdot\hat{s}_3 = i\Gamma_{3,1,2}A_1(\vec{r})A_2(\vec{r})e^{i(\vec{k}_1+\vec{k}_2-\vec{k}_3)\cdot\vec{r}}, \tag{12}$$

with coupling coefficient

$$\begin{aligned}\Gamma_{3,1,2} = \omega_3\big[&\bar{\bar{\chi}}^{(2)}_{eee} : \vec{e}_1\vec{e}_2\cdot\vec{e}^*_3 + \bar{\bar{\chi}}^{(2)}_{eme} : \vec{h}_1\vec{e}_2\cdot\vec{e}^*_3 \\ &+ \bar{\bar{\chi}}^{(2)}_{eem} : \vec{e}_1\vec{h}_2\cdot\vec{e}^*_3 + \bar{\bar{\chi}}^{(2)}_{emm} : \vec{h}_1\vec{h}_2\cdot\vec{e}^*_3 \\ &+ \bar{\bar{\chi}}^{(2)}_{mee} : \vec{e}_1\vec{e}_2\cdot\vec{h}^*_3 + \bar{\bar{\chi}}^{(2)}_{mme} : \vec{h}_1\vec{e}_2\cdot\vec{h}^*_3 \\ &+ \bar{\bar{\chi}}^{(2)}_{mem} : \vec{e}_1\vec{h}_2\cdot\vec{h}^*_3 + \bar{\bar{\chi}}^{(2)}_{mmm} : \vec{h}_1\vec{h}_2\cdot\vec{h}^*_3\big].\end{aligned} \tag{13}$$

B. Coupled-mode equations for wave-mixing processes in a periodic medium

We consider a MM as being formed from an inclusion that is infinitely repeated in three dimensions. For such a periodic medium, the wave equation admits solutions in the form of Bloch modes indexed by the Bloch wave vector $\vec{k}$. When the wavelength is much larger than the inclusion size and lattice constant, it becomes useful to average over the local fields and parameters associated with the inclusions, arriving at a set of macroscopic fields that are defined only at the edges and faces of the unit cells. These fields thus naturally satisfy a set of finite-difference equations, which, in the limit of weak nonlinearity, can be extended using coupled-mode theory to describe the fields resulting from wave-mixing processes, such

as second-harmonic generation (SHG), sum-frequency generation (SFG), and difference-frequency generation (DFG).

We can model our MM as an infinite medium described by a periodic relative permittivity $\epsilon(\vec{r})$ and second-order electric nonlinearity $\chi^{(2)}_{loc}(\vec{r})$, with implicit frequency dependencies. For simplicity, we will assume the unit cell is cubic with lattice constant a and primitive lattice vectors oriented along the three Cartesian axes, such that $\epsilon(\vec{r}) = \epsilon(\vec{r} + \vec{R})$ for lattice vector $\vec{R} = (n_1\hat{x} + n_2\hat{y} + n_3\hat{z})a$, where n_1, n_2, and n_3 are integers. Thus, the electric and magnetic fields corresponding to a particular Bloch mode μ can be written as

$$\begin{aligned}\vec{E}_\mu(\vec{r}) &= A_\mu \vec{e}_\mu(\vec{r}) \exp(i\vec{k}_\mu \cdot \vec{r}),\\ \vec{H}_\mu(\vec{r}) &= A_\mu \vec{h}_\mu(\vec{r}) \exp(i\vec{k}_\mu \cdot \vec{r}),\end{aligned} \tag{14}$$

where A_μ is the mode amplitude, k_μ is the Bloch wave vector, and $\vec{e}_\mu(\vec{r})$ and $\vec{h}_\mu(\vec{r})$ are periodic electric and magnetic Bloch functions, respectively, with the same periodicity as the MM lattice. The Bloch solutions form an orthogonal set of functions [60], allowing us to treat the Bloch modes in analogy to guided modes in coupled-mode theory [58,59]. Moreover, we assume that only the fundamental or lowest Bloch modes play a significant role in wave propagation and scattering, as is usual for MMs.

At this point, it is appropriate to apply several constraints to the total fields in the presence of the perturbation. Since our goal is characterization of the effective nonlinear tensors, it is desirable to probe the elements of these tensors independently. Thus, at any time, we will consider only the subset of modes necessary to probe a single tensor element of each susceptibility, that is, just three modes with specified frequencies, polarizations, and propagation directions. This is very similar to what is done in linear retrieval methods [52], and is often enforced in simulations by appropriate boundary conditions. Thus, we derive the rate equations for a particular Bloch mode with frequency ω_3, driven by Bloch modes at ω_1 and ω_2, such that $\omega_1 + \omega_2 = \omega_3$. Finally, we assume a sufficiently weak nonlinearity so that the mode amplitudes are slowly varying over a unit cell, allowing us to expand the fields *within* a unit cell in terms of the Bloch modes of the periodic, linear medium.

As before, we start by considering propagating modes at three distinct frequencies, whose coupling in the presence of a weak perturbation can be described by Eq. (A9). Using the relations in (14), this gives

$$\begin{aligned}&\nabla \cdot \{A_\mu[\vec{e}_3(\vec{r}) \times \vec{h}_3(\vec{r})^* + \vec{e}_3(\vec{r})^* \times \vec{h}_3(\vec{r})]\}\\ &\quad = i\omega_3[\vec{P}^{(2)}(\vec{r}) \cdot \vec{e}_3(\vec{r})^* + \vec{M}^{(2)}(\vec{r}) \cdot \vec{h}_3(\vec{r})^*]e^{-i\vec{k}_3\cdot\vec{r}}.\end{aligned} \tag{15}$$

Since we are considering MMs composed of purely electrically polarizable materials, $\vec{M}^{(2)}(\vec{r})$ can be neglected, while the second-order polarization is given by

$$\vec{P}^{(2)}(\vec{r}) = 2A_1A_2\bar{\bar{\chi}}^{(2)}_{loc}(\vec{r}) : \vec{e}_1(\vec{r})\vec{e}_2(\vec{r})e^{i(\vec{k}_1+\vec{k}_2)\cdot\vec{r}}. \tag{16}$$

However, a similar procedure can be employed for MMs composed of intrinsically magnetic materials.

Due to the inhomogeneous nature of the MM, the Bloch modes may contain rapidly varying fields that are generally unimportant in terms of predicting wave scattering behavior. It is thus convenient to average these rapidly varying field components over a unit cell, and instead follow the behavior of slowly varying (or macroscopic) fields at a discrete number of points that form a lattice with dimension a. So long as $a \ll \lambda$, the discreteness of the lattice is not of significance, though effects due to spatial dispersion may enter, especially near material resonances (see Sec. V).

The integral formulation of coupled-mode theory lends itself naturally to this type of averaging. Moreover, for the Bloch modes defined in (14), it is natural to consider the mode amplitudes A_μ as slowly varying envelopes in the presence of the nonlinear perturbation, while the rapid variations in field induced by local inhomogeneity are completely contained within the Bloch functions $\vec{e}_\mu(\vec{r})$ and $\vec{h}_\mu(\vec{r})$. Thus, we switch to the integral form of Eq. (A9) and allow the mode amplitudes to vary explicitly with the spatial coordinates $\vec{r}$, yielding

$$\begin{aligned}&\iiint_{V_0} \nabla \cdot \{A_3(\vec{r})[\vec{e}_3(\vec{r}) \times \vec{h}_3(\vec{r})^* + \vec{e}_3(\vec{r})^* \times \vec{h}_3(\vec{r})]\}dV\\ &\quad = 2i\omega_3 \iiint_{V_0} [A_1(\vec{r})A_2(\vec{r})\bar{\bar{\chi}}^{(2)}_{loc}(\vec{r}) : \vec{e}_1(\vec{r})\vec{e}_2(\vec{r})\\ &\qquad \cdot \vec{e}_3(\vec{r})^*]e^{i(\vec{k}_1+\vec{k}_2-\vec{k}_3)\cdot\vec{r}}dV,\end{aligned} \tag{17}$$

where the volume V_0 is taken to be a single unit cell, centered about the origin $\mathbf{0}$. We can distribute the divergence operator on the left-hand side, yielding

$$\begin{aligned}&\iiint_{V_0} \nabla \cdot \{A_3(\vec{r})[\vec{e}_3(\vec{r}) \times \vec{h}_3(\vec{r})^* + \vec{e}_3(\vec{r})^* \times \vec{h}_3(\vec{r})]\}dV\\ &= \iiint_{V_0} \nabla A_3(\vec{r}) \cdot [\vec{e}_3(\vec{r}) \times \vec{h}_3(\vec{r})^* + \vec{e}_3(\vec{r})^* \times \vec{h}_3(\vec{r})]dV\\ &\quad + \iiint_{V_0} A_3(\vec{r})\nabla \cdot [\vec{e}_3(\vec{r}) \times \vec{h}_3(\vec{r})^* + \vec{e}_3(\vec{r})^* \times \vec{h}_3(\vec{r})]dV.\end{aligned} \tag{18}$$

The integrand of the second term on the left-hand side vanishes identically, since it is proportional to the divergence of the Poynting vector of an unperturbed mode, leaving only the term proportional to $\nabla A_3(\vec{r})$. Invoking the slowly varying amplitude approximation, we can expand $\nabla A_3(\vec{r})$ about the origin in a Taylor series. Keeping only the lowest-order term, we thus replace (17) with the approximate equation

$$\begin{aligned}&\nabla A_3(\mathbf{0}) \cdot \iiint_{V_0} [\vec{e}_3(\vec{r}) \times \vec{h}_3(\vec{r})^* + \vec{e}_3(\vec{r})^* \times \vec{h}_3(\vec{r})]dV\\ &\quad \approx 2i\omega_3 \iiint_{V_0} [A_1(\vec{r})A_2(\vec{r})\bar{\bar{\chi}}^{(2)}_{loc}(\vec{r}) : \vec{e}_1(\vec{r})\vec{e}_2(\vec{r})\\ &\qquad \cdot \vec{e}_3(\vec{r})^*]e^{i(\vec{k}_1+\vec{k}_2-\vec{k}_3)\cdot\vec{r}}dV.\end{aligned} \tag{19}$$

Written this way, the integral on the left-hand side resembles the volume averaged Poynting vector for the unperturbed mode. Consistent with the homogeneous coupled-wave formalism, we introduce the normalization condition

$$\frac{1}{2a^3}\iiint_{V_0} [\vec{e}_\mu(\vec{r}) \times \vec{h}_\mu(\vec{r})^* + \vec{e}_\mu(\vec{r})^* \times \vec{h}_\mu(\vec{r})]dV = \hat{s}_\mu, \tag{20}$$

such that $\hat{s}_\mu$ represents the unit normal in the direction of the averaged Poynting vector for the unperturbed mode μ.

In order to reduce the right-hand side of Eq. (19), we similarly expand the fundamental mode amplitudes in a Taylor series, and again, invoking the slowly varying amplitude

approximation, keep only the lowest-order terms. Thus, we arrive at the following relation:

$$\nabla A_3(\mathbf{0}) \cdot \hat{s}_3 = i\Gamma_{3,1,2} A_1(\mathbf{0}) A_2(\mathbf{0}), \tag{21}$$

with coupling coefficients

$$\Gamma_{3,1,2} = \frac{\omega_3}{a^3} \iiint_{V_0} \left[\bar{\bar{\chi}}^{(2)}_{loc}(\vec{r}) : \vec{e}_1(\vec{r})\vec{e}_2(\vec{r}) \cdot \vec{e}^*_3(\vec{r}) e^{i(\vec{k}_1+\vec{k}_2-\vec{k}_3)\cdot\vec{r}}\right] dV. \tag{22}$$

We can then describe the coupling at any unit cell in the infinite lattice by translating Eq. (21) by lattice vector $\vec{R}$, yielding

$$\nabla A_3(\vec{R}) \cdot \hat{s}_3 = i\Gamma_{3,1,2} A_1(\vec{R}) A_2(\vec{R}) e^{i(\vec{k}_1+\vec{k}_2-\vec{k}_3)\cdot\vec{R}}. \tag{23}$$

Due to the periodicity of the Bloch functions and local material properties, the coupling coefficient $\Gamma_{3,1,2}$ is invariant to the unit cell at which it is defined, and effectively replaces the homogeneous nonlinear susceptibility of the previous section. In other words, Eq. (24) gives an approximate relation for the rate of change of wave 3 in the direction of energy flow, proportional to the product of the fundamental wave amplitudes, the momenta mismatch, and an averaged coupling coefficient, on a discrete lattice that is defined by the MM's own structural periodicity.

The form of Eq. (23) is easily converted to a finite-difference system of equations by replacing the gradient with an appropriate finite-difference approximation. Alternatively, in the limit $a \to 0$, we can take $\vec{R} \to \vec{r}$, and thus Eq. (23) approaches the continuous form

$$\nabla A_3(\vec{r}) \cdot \hat{s}_3 = i\Gamma_{3,1,2} A_1(\vec{r}) A_2(\vec{r}) e^{i(\vec{k}_1+\vec{k}_2-\vec{k}_3)\cdot\vec{r}}, \tag{24}$$

as expected. It is clear that, from such a perspective, the detailed MM structure can be largely ignored once $\Gamma_{3,1,2}$ is obtained. Thus, the coupled-mode equations for a nonlinear MM, within the limits discussed above, are largely indistinguishable from the coupled-wave equations for a homogeneous nonlinear medium.

C. The effective second-order susceptibilities

In this section, we combine the results of the previous two sections to arrive at expressions for the eight constitutive second-order susceptibilities describing the nonlinear MM as a homogeneous medium. As is the usual case for homogenization of MMs, we require that the behavior of a single unit cell be perfectly replicated by an equivalent slab of homogeneous material. To simplify the analysis, we will use the continuous forms of the nonlinear coupling in both cases, thus implying the limit $a \to 0$ on the resulting equations. The more general form will be handled in Sec. V. Moreover, we will consider the special case where the three Bloch modes propagate along the z axis, with macroscopic electric fields polarized along the x axis, and macroscopic magnetic fields polarized along the y axis, so that, from the homogeneous perspective, the equations become scalar.

From inspection of the terms in Eqs. (12) and (24), homogenization requires two steps. First, we must establish equivalence in the linear wave propagation between the homogeneous and MM systems, consisting of the particular wave vectors and associated fields. Thus, we invoke standard eigenfrequency analyses to establish the wave vectors and Bloch functions in the periodic medium. Consistent with Smith and Pendry's field-averaging method [52], the macroscopic electric and magnetic fields of our homogeneous system, then, are given by line integrals along the borders of the unit cell. This gives us the following relation between macroscopic and local electric fields:

$$\tilde{e}_\mu = \frac{1}{a}\int_{-\frac{a}{2}}^{+\frac{a}{2}} \left[\vec{e}_\mu\left(x, \pm\frac{a}{2}, \pm\frac{a}{2}\right)\cdot\hat{x}\right] dx, \tag{25}$$

where the tilde is used to denote a macroscopic quantity. The macroscopic magnetic field is likewise defined by

$$\tilde{h}_\mu = \frac{1}{a}\int_{-\frac{a}{2}}^{+\frac{a}{2}} \left[\vec{h}_\mu\left(\pm\frac{a}{2}, y, \pm\frac{a}{2}\right)\cdot\hat{y}\right] dy. \tag{26}$$

From here, we can define the wave impedance for mode μ as

$$Z_\mu = \frac{\tilde{e}_\mu}{\tilde{h}_\mu}. \tag{27}$$

Second, we must establish equivalence in the nonlinear behavior between the MM and homogeneous mediums. In the limit $a \to 0$, the nonlinear behavior is completely embodied by the coupling coefficients given in (13) and (22). Thus, substituting the macroscopic fields defined above into (13), we equate (13) and (22) and cancel the like terms to find

$$\begin{aligned}
&\frac{1}{a^3}\iiint_{V_0}\left[\bar{\bar{\chi}}^{(2)}_{loc}(\vec{r}) : \vec{e}_1(\vec{r})\vec{e}_2(\vec{r})\cdot\vec{e}^*_3(\vec{r}) e^{i(k_1+k_2-k_3)z}\right] dV \\
&= \left[\chi^{(2)}_{eee}\tilde{e}_1\tilde{e}_2\tilde{e}^*_3 + \chi^{(2)}_{eme}\tilde{h}_1\tilde{e}_2\tilde{e}^*_3 + \chi^{(2)}_{eem}\tilde{e}_1\tilde{h}_2\tilde{e}^*_3\right. \\
&\quad + \chi^{(2)}_{emm}\tilde{h}_1\tilde{h}_2\tilde{e}^*_3 + \chi^{(2)}_{mee}\tilde{e}_1\tilde{e}_2\tilde{h}^*_3 + \chi^{(2)}_{mme}\tilde{h}_1\tilde{e}_2\tilde{h}^*_3 \\
&\quad \left. + \chi^{(2)}_{mem}\tilde{e}_1\tilde{h}_2\tilde{h}^*_3 + \chi^{(2)}_{mmm}\tilde{h}_1\tilde{h}_2\tilde{h}^*_3\right].
\end{aligned} \tag{28}$$

However, this single equation is not enough to solve for the eight as-yet-undetermined second-order susceptibilities. To introduce additional equations while still probing the same effective tensor elements, we note that all of the forward propagating modes considered up to now must have a conjugate mode that propagates in the opposite direction. The above expressions, moreover, are easily extended to allow for modes propagating in either the positive or negative z directions. Enforcing equality for *each* combination of modes independently, i.e., eight in total, we obtain a system of eight equations that can be written in compact form as

$$\begin{aligned}
&\frac{1}{a^3}\iiint_{V_0}\left[\bar{\bar{\chi}}^{(2)}_{loc}(\vec{r}) : \vec{e}_\rho(\vec{r})\vec{e}_\psi(\vec{r})\cdot\vec{e}^*_\nu(\vec{r}) e^{i(k_\rho+k_\psi-k_\nu)z}\right] dV \\
&= \left[\chi^{(2)}_{eee}\tilde{e}_\rho\tilde{e}_\psi\tilde{e}^*_\nu + \chi^{(2)}_{eme}\tilde{h}_\rho\tilde{e}_\psi\tilde{e}^*_\nu + \chi^{(2)}_{eem}\tilde{e}_\rho\tilde{h}_\psi\tilde{e}^*_\nu\right. \\
&\quad + \chi^{(2)}_{emm}\tilde{h}_\rho\tilde{h}_\psi\tilde{e}^*_\nu + \chi^{(2)}_{mee}\tilde{e}_\rho\tilde{e}_\psi\tilde{h}^*_\nu + \chi^{(2)}_{mme}\tilde{h}_\rho\tilde{e}_\psi\tilde{h}^*_\nu \\
&\quad \left. + \chi^{(2)}_{mem}\tilde{e}_\rho\tilde{h}_\psi\tilde{h}^*_\nu + \chi^{(2)}_{mmm}\tilde{h}_\rho\tilde{h}_\psi\tilde{h}^*_\nu\right],
\end{aligned} \tag{29}$$

for all combinations of $\nu = \pm 3$, $\rho = \pm 1$, and $\psi = \pm 2$, where a negative sign denotes a mode with identical frequency and polarization but propagating in the negative z direction. The eight equations represented by (29) contain the eight undetermined effective nonlinearities and, in the most general case, can be solved by linear algebra.

This set of equations can be further simplified if we assume the unit cell's linear local material properties are purely real,

that is, there is no loss or gain in the system. In this case, the symmetry in the Bloch wave equation allows us to write the backward Bloch modes directly from the forward Bloch modes at the same frequency, such that

$$\vec{e}_{-n}(\vec{r}) = \vec{e}_n^*(\vec{r}) \quad \text{and} \quad \vec{h}_{-n}(\vec{r}) = -\vec{h}_n^*(\vec{r}), \tag{30}$$

for $n = 1,2,3$. Together with Eq. (27) and normalization condition (20), this implies $\tilde{e}_{\pm n} = \sqrt{Z_n}$ and $\tilde{h}_{\pm n} = \pm 1/\sqrt{Z_n}$.

Using these relations in (29), the equations can be rearranged to solve for the effective second-order susceptibilities in closed form, finally yielding the following expressions for the effective electric, magnetic, and magnetoelectric nonlinear susceptibilities:

$$\chi^{(2)}_{eee}(\omega_3;\omega_1,\omega_2) = \frac{1}{a^3}\iiint_{V_0} dV\left[\bar{\bar{\chi}}^{(2)}_{loc}(\vec{r}) : \vec{\theta}_1(\vec{r})\vec{\theta}_2(\vec{r})\cdot\vec{\theta}_3(\vec{r})\right], \tag{31}$$

$$\chi^{(2)}_{emm}(\omega_3;\omega_1,\omega_2) = -\frac{1}{a^3}\iiint_{V_0} dV\left[\bar{\bar{\chi}}^{(2)}_{loc}(\vec{r}) : \vec{\phi}_1(\vec{r})\vec{\phi}_2(\vec{r})\cdot\vec{\theta}_3(\vec{r})\right], \tag{32}$$

$$\chi^{(2)}_{eem}(\omega_3;\omega_1,\omega_2) = \frac{i}{a^3}\iiint_{V_0} dV\left[\bar{\bar{\chi}}^{(2)}_{loc}(\vec{r}) : \vec{\theta}_1(\vec{r})\vec{\phi}_2(\vec{r})\cdot\vec{\theta}_3(\vec{r})\right], \tag{33}$$

$$\chi^{(2)}_{eme}(\omega_3;\omega_1,\omega_2) = \frac{i}{a^3}\iiint_{V_0} dV\left[\bar{\bar{\chi}}^{(2)}_{loc}(\vec{r}) : \vec{\phi}_1(\vec{r})\vec{\theta}_2(\vec{r})\cdot\vec{\theta}_3(\vec{r})\right], \tag{34}$$

$$\chi^{(2)}_{mmm}(\omega_3;\omega_1,\omega_2) = \frac{i}{a^3}\iiint_{V_0} dV\left[\bar{\bar{\chi}}^{(2)}_{loc}(\vec{r}) : \vec{\phi}_1(\vec{r})\vec{\phi}_2(\vec{r})\cdot\vec{\phi}_3(\vec{r})\right], \tag{35}$$

$$\chi^{(2)}_{mee}(\omega_3;\omega_1,\omega_2) = -\frac{i}{a^3}\iiint_{V_0} dV\left[\bar{\bar{\chi}}^{(2)}_{loc}(\vec{r}) : \vec{\theta}_1(\vec{r})\vec{\theta}_2(\vec{r})\cdot\vec{\phi}_3(\vec{r})\right], \tag{36}$$

$$\chi^{(2)}_{mme}(\omega_3;\omega_1,\omega_2) = \frac{1}{a^3}\iiint_{V_0} dV\left[\bar{\bar{\chi}}^{(2)}_{loc}(\vec{r}) : \vec{\phi}_1(\vec{r})\vec{\theta}_2(\vec{r})\cdot\vec{\phi}_3(\vec{r})\right], \tag{37}$$

$$\chi^{(2)}_{mem}(\omega_3;\omega_1,\omega_2) = \frac{1}{a^3}\iiint_{V_0} dV\left[\bar{\bar{\chi}}^{(2)}_{loc}(\vec{r}) : \vec{\theta}_1(\vec{r})\vec{\phi}_2(\vec{r})\cdot\vec{\phi}_3(\vec{r})\right], \tag{38}$$

where we have introduced the quantities

$$\vec{\theta}_n(\vec{r}) = \frac{1}{2}\left[\frac{\vec{e}_n(\vec{r})}{\tilde{e}_n}e^{ik_n z} + \frac{\vec{e}_{-n}(\vec{r})}{\tilde{e}_{-n}}e^{-ik_n z}\right] = \mathrm{Re}\left[\frac{\vec{e}_n(\vec{r})}{\tilde{e}_n}e^{ik_n z}\right] \tag{39}$$

$$\text{and} \quad \vec{\phi}_n(\vec{r}) = \frac{1}{2i}\left[\frac{\vec{e}_n(\vec{r})}{\tilde{h}_n}e^{ik_n z} + \frac{\vec{e}_{-n}(\vec{r})}{\tilde{h}_{-n}}e^{-ik_n z}\right] = \mathrm{Im}\left[\frac{\vec{e}_n(\vec{r})}{\tilde{h}_n}e^{ik_n z}\right]. \tag{40}$$

These final forms for the second-order susceptibility can be understood from an intuitive, if informal, perspective, by considering $\vec{\theta}_n(\vec{r})$ and $\vec{\phi}_n(\vec{r})$ as standing-wave patterns. From a macroscopic perspective, $\vec{\theta}_n(\vec{r})$ corresponds to a standing-wave distribution with an electric field antinode at the unit-cell center. $\vec{\phi}_n(\vec{r})$ is then the electric field distribution corresponding to a macroscopic magnetic field antinode at the unit-cell center. Thus, by specifying the dominant *macroscopic* fields, the appropriate nonlinearity can be related quite naturally to the corresponding *microscopic* fields. In this way, the macroscopic field symmetries are enforced in the local response, such that the homogenized nonlinearities are unambiguous. As an example, typical plots of $\vec{\theta}(\vec{r})$ and $\vec{\phi}(\vec{r})$ are shown in Fig. 1 for a MM consisting of high-dielectric spheres, obtained from eigenfrequency simulations.

This final result for the effective second-order magnetoelectric susceptibilities is very satisfying and highly intuitive. By rearranging the Bloch modes, we are able to describe the local electric fields that are, from a macroscopic perspective, either electrically or magnetically induced. The effective response is completely characterized by the overlap of these local field distributions within the nonlinear component of the unit cell. In short, Eqs. (31)–(38) reveal that, as expected, clever structuring of MM inclusions can give rise to complex macroscopic nonlinear behaviors of a *fundamentally different nature* than the constituents.

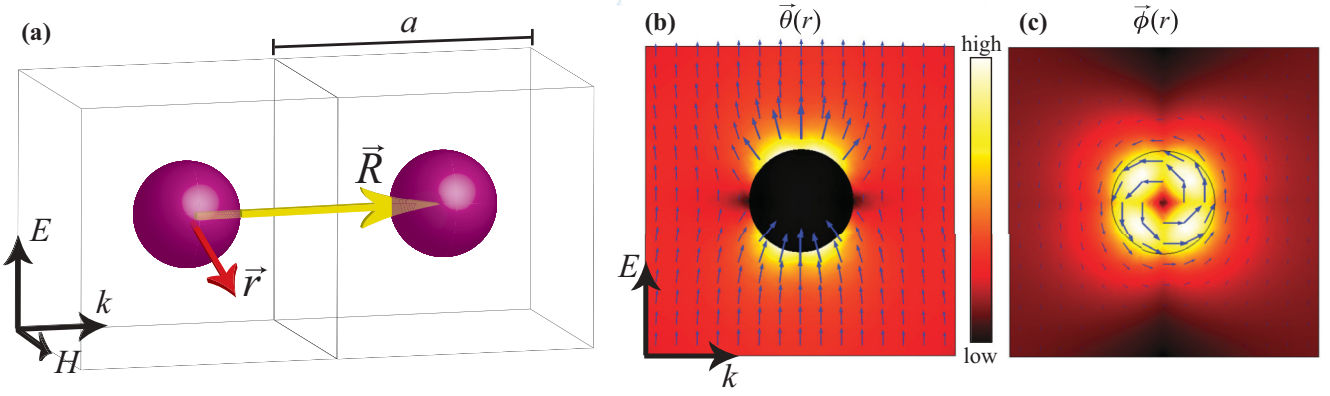

FIG. 1. (Color online) (a) The unit cell of an example MM composed of high-dielectric spheres, illustrating the coordinate ($\vec{r}$) and lattice ($\vec{R}$) vectors. (b) and (c) represent typical cross sections of $\vec{\theta}(\vec{r})$ and $\vec{\phi}(\vec{r})$, respectively, obtained from eigenfrequency simulations for spheres with $\epsilon/\epsilon_0 = 300$ and diameter $a/3$ embedded in free space, showing the expected electric- and magnetic-type responses.

The above analysis assumed propagation along the z axis for simplicity, as well as a homogenized medium whose normal modes, in the linear regime, are linearly polarized plane waves. Thus, while the effective nonlinear susceptibilities are themselves tensors, the above procedure only probes a single element of each tensor, determined by the polarizations of the macroscopic waves, i.e., the $\chi^{(2)}_{eee}$ in the above formalism is actually $\chi^{(2)}_{eee,xxx}$, $\chi^{(2)}_{mmm}$ is $\chi^{(2)}_{mmm,yyy}$, etc. However, even if the local nonlinearity is diagonal, the subwavelength structure of the MM can give rise to overlap between the different polarizations and thus nonzero cross terms in the effective tensors [32,61]. To recover the other elements of the susceptibility tensors, the polarization and direction of each wave can be manipulated successively, and the above procedure repeated independently for each tensor element. Additionally, if the normal modes of the linear homogenized medium cannot be decomposed into linearly polarized plane waves, as is the case, for example, in chiral MMs, an appropriate basis for homogenization, with well-defined wave impedances and wave vectors, should be used instead.

We note here that the decision to write the equations of motion for the fields at ω_3 is an arbitrary one. However, certain permutation symmetries and self-consistencies are readily found in the above expressions. Assuming $\omega_3 > \omega_2 > \omega_1 > 0$, permutation of the fundamental waves gives the same effective nonlinearity, i.e., $\chi^{(2)}_{eme}(\omega_3;\omega_1,\omega_2) = \chi^{(2)}_{eem}(\omega_3;\omega_2,\omega_1)$. Additionally, the complementary nonlinearities, by which we mean the nonlinearities describing the three-wave mixing process at the fundamental frequencies, are the conjugate of the first, i.e., $\chi^{(2)}_{eme}(\omega_3;\omega_1,\omega_2) = [\chi^{(2)}_{mee}(\omega_1;\omega_3,-\omega_2)]^* = [\chi^{(2)}_{eem}(\omega_2;\omega_3,-\omega_1)]^*$, where we have used the constraint of real total fields to relate the negative and positive frequency components. These properties of the nonlinear susceptibilities can be shown to ensure the proper photon and energy conservation requirements, as in the Manley-Rowe relations [37].

Finally, it is also worth noting that the units of the second-order susceptibilities are not all the same, but have been chosen to ensure the permutation symmetries discussed above. As seen in Eq. (13), each nonlinear susceptibility enters the equation for the coupling coefficient with a different leading coefficient, related to the wave impedances at the involved frequencies. Using Eq. (27), it is convenient to define individual coupling coefficients,

$$\gamma_{g_3g_1g_2} = \omega_3\sqrt{G_1G_2G_3}\,\chi^{(2)}_{g_3g_1g_2}, \tag{41}$$

where $G_n = Z_n$ for $g_n = e$, and $G_n = Y_n = 1/Z_n$ for $g_n = m$, such that

$$\begin{aligned}\Gamma_{\nu,\rho,\psi} = {}& \gamma^{(2)}_{eee} + \mathrm{sgn}(\rho)\gamma^{(2)}_{eme} + \mathrm{sgn}(\psi)\gamma^{(2)}_{eem} + \mathrm{sgn}(\rho\psi)\gamma^{(2)}_{emm} \\ & + \mathrm{sgn}(\nu)\gamma^{(2)}_{mee} + \mathrm{sgn}(\rho\nu)\gamma^{(2)}_{mme} + \mathrm{sgn}(\psi\nu)\gamma^{(2)}_{mem} \\ & + \mathrm{sgn}(\rho\psi\nu)\gamma^{(2)}_{mmm},\end{aligned} \tag{42}$$

where sgn() is the signum function. The eight individual coupling coefficients have units of $\mathrm{m}^{-1}(\mathrm{W/m^2})^{-1/2}$, and provide a means for direct comparison of the relative magnitudes and phases of the various second-order susceptibilities. Also, it is worth noting that the contributions from each nonlinearity to $\Gamma_{\nu,\rho,\psi}$ are uniquely dependent on the propagation directions of the three waves, denoted in our convention by the sign of the subscripts: a fact responsible for interesting interference effects in the presence of multiple nonlinearities, as discussed in Sec. IV A.

D. The effective third-order susceptibilities

Analogous to the second-order material responses of Eqs. (3) and (4), let us consider a third-order polarization and magnetization of the form

$$\begin{aligned}\vec{P}^{(3)}(t) = \sum_{pqr}\big[& \bar{\bar{\chi}}^{(3)}_{eeee}(\omega_s;\omega_p,\omega_q,\omega_r)\vdots\vec{E}(\omega_p)\vec{E}(\omega_q)\vec{E}(\omega_r) + \bar{\bar{\chi}}^{(3)}_{eemm}(\omega_s;\omega_p,\omega_q,\omega_r)\vdots\vec{E}(\omega_p)\vec{H}(\omega_q)\vec{H}(\omega_r) \\ & + \bar{\bar{\chi}}^{(3)}_{eeem}(\omega_s;\omega_p,\omega_q,\omega_r)\vdots\vec{E}(\omega_p)\vec{E}(\omega_q)\vec{H}(\omega_r) + \bar{\bar{\chi}}^{(3)}_{eeme}(\omega_s;\omega_p,\omega_q,\omega_r)\vdots\vec{E}(\omega_p)\vec{H}(\omega_q)\vec{E}(\omega_r) \\ & + \bar{\bar{\chi}}^{(3)}_{emee}(\omega_s;\omega_p,\omega_q,\omega_r)\vdots\vec{H}(\omega_p)\vec{E}(\omega_q)\vec{E}(\omega_r) + \bar{\bar{\chi}}^{(3)}_{emmm}(\omega_s;\omega_p\omega_q,\omega_r)\vdots\vec{H}(\omega_p)\vec{H}(\omega_q)\vec{H}(\omega_r) \\ & + \bar{\bar{\chi}}^{(3)}_{emem}(\omega_s;\omega_p,\omega_q,\omega_r)\vdots\vec{H}(\omega_p)\vec{E}(\omega_q)\vec{H}(\omega_r) + \bar{\bar{\chi}}^{(3)}_{emme}(\omega_s;\omega_p,\omega_q,\omega_r)\vdots\vec{H}(\omega_p)\vec{H}(\omega_q)\vec{E}(\omega_r)\big]\exp(-i\omega_s t),\end{aligned} \tag{43}$$

$$\begin{aligned}\mu_0\vec{M}^{(3)}(t) = \sum_{pqr}\big[& \bar{\bar{\chi}}^{(3)}_{mmmm}(\omega_s;\omega_p,\omega_q,\omega_r)\vdots\vec{H}(\omega_p)\vec{H}(\omega_q)\vec{H}(\omega_r) + \bar{\bar{\chi}}^{(3)}_{mmee}(\omega_s;\omega_p,\omega_q,\omega_r)\vdots\vec{H}(\omega_p)\vec{E}(\omega_q)\vec{E}(\omega_r) \\ & + \bar{\bar{\chi}}^{(3)}_{mmme}(\omega_s;\omega_p,\omega_q,\omega_r)\vdots\vec{H}(\omega_p)\vec{H}(\omega_q)\vec{E}(\omega_r) + \bar{\bar{\chi}}^{(3)}_{mmem}(\omega_s;\omega_p,\omega_q,\omega_r)\vdots\vec{H}(\omega_p)\vec{E}(\omega_q)\vec{H}(\omega_r) \\ & + \bar{\bar{\chi}}^{(3)}_{memm}(\omega_s;\omega_p,\omega_q,\omega_r)\vdots\vec{E}(\omega_p)\vec{H}(\omega_q)\vec{H}(\omega_r) + \bar{\bar{\chi}}^{(3)}_{meee}(\omega_s;\omega_p,\omega_q,\omega_r)\vdots\vec{E}(\omega_p)\vec{E}(\omega_q)\vec{E}(\omega_r) \\ & + \bar{\bar{\chi}}^{(3)}_{meme}(\omega_s;\omega_p,\omega_q,\omega_r)\vdots\vec{E}(\omega_p)\vec{H}(\omega_q)\vec{E}(\omega_r) + \bar{\bar{\chi}}^{(3)}_{meem}(\omega_s;\omega_p,\omega_q,\omega_r)\vdots\vec{E}(\omega_p)\vec{E}(\omega_q)\vec{H}(\omega_r)\big]\exp(-i\omega_s t),\end{aligned} \tag{44}$$

where $\sum_{pqr}$ denotes a triple sum, and $\omega_s = \omega_p + \omega_q + \omega_r$, thus defining 16 third-order susceptibility tensors of rank 4. The same procedure as in the previous section can be carried out for four-wave mixing in a MM composed of a periodic electric third-order susceptibility, $\bar{\bar{\chi}}^{(3)}_{loc}(\vec{r})$. This gives a system of 16 equations relating the microscopic Bloch field distributions to the

16 macroscopic susceptibilities, represented by

$$\frac{1}{a^3}\iiint_{V_0} dV\left[\bar{\bar{\chi}}^{(3)}_{loc}(\vec{r}):\vec{e}_\rho(\vec{r})\vec{e}_\psi(\vec{r})\vec{e}_\zeta(\vec{r})\cdot\vec{e}^*_\nu(\vec{r})\right]$$
$$= \chi^{(3)}_{eeee}\tilde{e}_\rho\tilde{e}_\psi\tilde{e}_\zeta\tilde{e}_\nu + \chi^{(3)}_{eeme}\tilde{e}_\rho\tilde{h}_\psi\tilde{e}_\zeta\tilde{e}_\nu + \chi^{(3)}_{eeem}\tilde{e}_\rho\tilde{e}_\psi\tilde{h}_\zeta\tilde{e}_\nu + \chi^{(3)}_{eemm}\tilde{e}_\rho\tilde{h}_\psi\tilde{h}_\zeta\tilde{e}_\nu + \chi^{(3)}_{meee}\tilde{e}_\rho\tilde{e}_\psi\tilde{e}_\zeta\tilde{h}_\nu + \chi^{(3)}_{meme}\tilde{e}_\rho\tilde{h}_\psi\tilde{e}_\zeta\tilde{h}_\nu$$
$$+ \chi^{(3)}_{meem}\tilde{e}_\rho\tilde{e}_\psi\tilde{h}_\zeta\tilde{h}_\nu + \chi^{(3)}_{memm}\tilde{e}_\rho\tilde{h}_\psi\tilde{h}_\zeta\tilde{h}_\nu + \chi^{(3)}_{emee}\tilde{h}_\rho\tilde{e}_\psi\tilde{e}_\zeta\tilde{e}_\nu + \chi^{(3)}_{emme}\tilde{h}_\rho\tilde{h}_\psi\tilde{e}_\zeta\tilde{e}_\nu + \chi^{(3)}_{emem}\tilde{h}_\rho\tilde{e}_\psi\tilde{h}_\zeta\tilde{e}_\nu + \chi^{(3)}_{emmm}\tilde{h}_\rho\tilde{h}_\psi\tilde{h}_\zeta\tilde{e}_\nu$$
$$+ \chi^{(3)}_{mmee}\tilde{h}_\rho\tilde{e}_\psi\tilde{e}_\zeta\tilde{h}_\nu + \chi^{(3)}_{mmme}\tilde{h}_\rho\tilde{h}_\psi\tilde{e}_\zeta\tilde{h}_\nu + \chi^{(3)}_{mmem}\tilde{h}_\rho\tilde{e}_\psi\tilde{h}_\zeta\tilde{h}_\nu + \chi^{(3)}_{mmmm}\tilde{h}_\rho\tilde{h}_\psi\tilde{h}_\zeta\tilde{h}_\nu, \quad (45)$$

for $\rho = \pm1$, $\psi = \pm2$, $\zeta = \pm3$, $\nu = \pm4$. As before, assuming lossless materials, 16 closed-form expressions can be derived for the effective third-order susceptibilities of the form

$$\chi^{(3)}_{eeme}(\omega_4;\omega_1,\omega_2,\omega_3) = \frac{i}{a^3}\iiint_{V_0} dV\left[\bar{\bar{\chi}}^{(3)}_{loc}(\vec{r}):\vec{\theta}_1(\vec{r})\vec{\phi}_2(\vec{r})\vec{\theta}_3(\vec{r})\cdot\vec{\theta}_4(\vec{r})\right]. \quad (46)$$

For brevity, and due to similarities with the second-order expressions, we will omit the equations for the 15 other third-order susceptibilities.

III. NUMERICAL EXAMPLES

According to (31)–(38), the eight homogenized nonlinear magnetoelectric susceptibilities can be evaluated directly from the Bloch modes at the three frequencies, found either analytically or numerically. Moreover, since the quantities in the denominators of (39) and (40) are explicitly derived from the numerators, the phases and amplitudes of $\vec{\theta}_n(\vec{r})$ and $\vec{\phi}_n(\vec{r})$ are automatically normalized, precluding the usual problems associated with ill-defined Bloch modes. Thus, when calculating the effective nonlinearities from numerical simulations, the computed Bloch modes can be used directly in (39) and (40), facilitating the homogenization process. Thus, the effective linear and nonlinear properties describing three-wave mixing in a MM can be characterized from the results of just three eigenfrequency simulations. In this section, we apply this procedure to several example MMs, demonstrating the ability of these structures to support electric, magnetic, and magnetoelectric second-order responses.

A. The split-ring resonator

In order to validate the above expressions for the second-order susceptibilities, we first apply the analysis to a well-researched nonlinear MM: the split-ring resonator (SRR). For simplicity, we assume the local second-order response of the SRR is zero everywhere except for a small dielectric slab loaded into the structure's capacitive gap, modeled by $\epsilon/\epsilon_0 = 25$ and $\chi^{(2)}_{loc,zzz}/\epsilon_0 = 1$ pm/V. The background dielectric is taken to be free space. To allow extrapolation over a wide range of frequencies, the SRR's dimensions, given in Fig. 2(a), are related to the lattice constant a, and the results are given as a function of normalized frequencies, $\omega_n a/2\pi c$. To validate the use of Eq. (30), dielectric losses are neglected, and the metal ring is modeled by a perfect electric conductor with thickness $a/100$. Using COMSOL MULTIPHYSICS, we employ eigenfrequency simulations on the unit cell to determine the lowest forward propagating Bloch modes and eigenfrequencies over a range of wave vectors, assuming the incident fields are polarized according to Fig. 2(a). In this way, we first determine the wave vectors and wave impedances as a function of frequency, according to Ref. [52]. From previous theoretical investigations [27], we know that, when excited by a fundamental frequency (FF) close to the magnetic resonance, SHG is mediated by the purely magnetic nonlinearity, $\chi^{(2)}_{mmm}$. Moreover, due to the small size and high permittivity of the nonlinear dielectric, the $\hat{z}$ component of

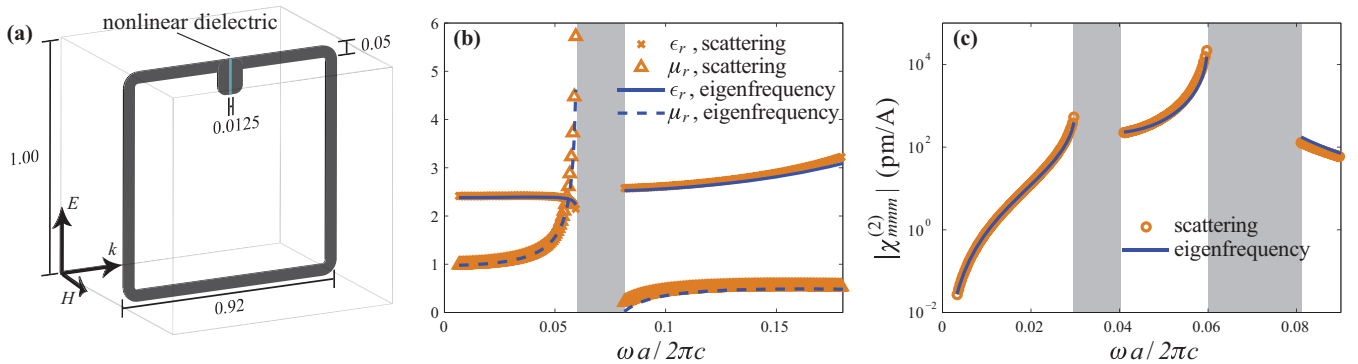

FIG. 2. (Color online) (a) Nonlinear SRR used in validating Eq. (35). Plots of the SRR's retrieved (b) linear and (c) nonlinear properties via both scattering and eigenfrequency simulations. The effective $\chi^{(2)}_{mmm}(2\omega;\omega,\omega)$ is retrieved by both the nonlinear transfer matrix method and Eq. (35), showing excellent agreement. The grayed frequency bands where no data is plotted correspond to either the FF or second-harmonic falling in the SRR's stop band that extends over a narrow range of frequencies above the magnetic resonance.

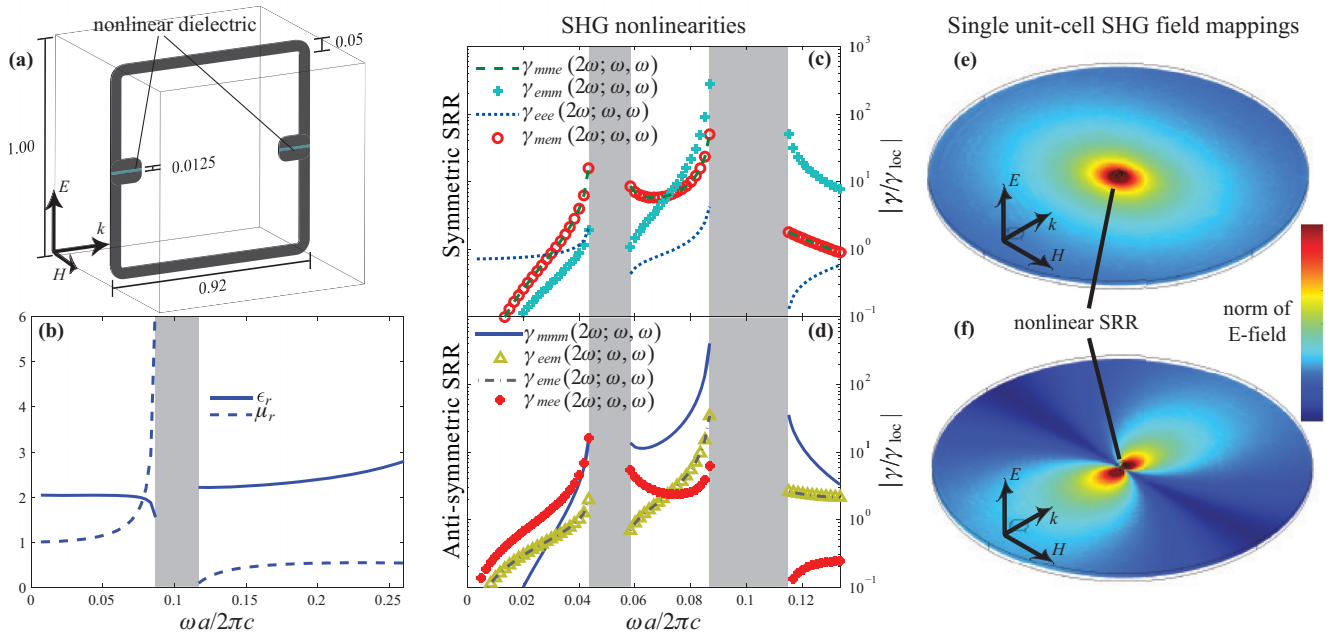

FIG. 3. (Color online) (a) The doubly-split nonlinear SRR used for both the symmetric and antisymmetric configurations. (b) The retrieved linear properties from eigenfrequency simulations. The second-order susceptibilities of the (c) symmetric and (d) antisymmetric SRRs for SHG, calculated via (31)–(38). Due to the degenerate frequencies involved in SHG, $\chi^{(2)}_{eem}$ and $\chi^{(2)}_{eme}$ are identical, as are $\chi^{(2)}_{mem}$ and $\chi^{(2)}_{mme}$. (e) and (f) show field maps of resonant SHG from infinite columns of symmetric and antisymmetric SRRs, respectively.

the electric field within the gap is nearly constant, allowing the integral in Eq. (35) to be approximated by the product of the average values of $\vec{\phi}_n$ within the gap and the nonlinear dielectric's volume. Thus, we record the eigenfrequency and $\vec{\phi}_n \cdot \hat{z}$ in the gap for a wide range of wave vectors, interpolating the results to determine $\chi^{(2)}_{mmm}(2\omega;\omega,\omega)$ as a function of the normalized FF $\omega a/2\pi c$, according to Eq. (35).

For comparison, we perform full-wave numerical simulations, using the existing nonlinear parameter retrieval method based on transfer matrices [48,62]. This method has been previously established for the retrieval of purely magnetic nonlinearities [47,63]. Thus, we retrieve the effective magnetic nonlinearity $\chi^{(2)}_{mmm}(2\omega;\omega,\omega)$ from nonlinear scattering simulations for a single unit cell with appropriate periodic boundary conditions. The linear properties are likewise determined from the linear scattering parameters [51]. The results of both retrieval techniques are presented in Figs. 2(b) and 2(c). The excellent agreement between the two methods lends validity to the procedure employed here. Small discrepancies between the two approaches can be attributed to the coupling between neighboring unit cells in the direction of propagation, neglected in the scattering simulations.

B. Prototypical nonlinear magnetoelectric metamaterial

Recently, nonlinear magnetoelectric coupling was demonstrated in a MM at microwave frequencies [49]. The MMs were varactor loaded split-ring resonators (VLSRRs), consisting of copper ring resonators with two capacitive gaps on either side. The varactor diodes provided the second-order response. Unlike the previous SRR, the gaps were oriented such that both electric *and* magnetic fields could excite voltages across the varactors, allowing nonlinear magnetoelectric coupling to take place.

Here, we analyze the analogous doubly-split ring resonator depicted in Fig. 3(a), in which the capacitive gaps are loaded with small nonlinear dielectric films, as in the previous example. The effective linear properties are obtained via field averaging and plotted in Fig. 3(b), showing the expected magnetic resonance. In terms of the nonlinear properties, we consider two structures, corresponding to orientation of the nonlinear dielectrics in the same direction (symmetric SRR) or in opposite directions (antisymmetric SRR). These configurations imply even and odd symmetries in the nonlinear properties with respect to the z coordinate, i.e., $\bar{\bar{\chi}}^{(2)}_{loc}(x,y,z) = \bar{\bar{\chi}}^{(2)}_{loc}(x,y,-z)$ and $\bar{\bar{\chi}}^{(2)}_{loc}(x,y,z) = -\bar{\bar{\chi}}^{(2)}_{loc}(x,y,-z)$, respectively. We follow the same procedure as before, but evaluating *all* of the second-order susceptibilities for both configurations. The magnitudes of the strongest four γ are plotted in Figs. 3(c) and 3(d), normalized by the value for a solid block of the nonlinear dielectric, γ_{loc}.

At the resonance frequency, we see the dominant nonlinear process to be $\chi^{(2)}_{mmm}(2\omega;\omega,\omega)$ in the antisymmetric SRR, and $\chi^{(2)}_{emm}(2\omega;\omega,\omega)$ in the symmetric SRR, in agreement with experiments on analogous VLSRRs [49]. The nature of these differing nonlinearities is further illustrated in Figs. 3(e) and 3(f), which give a cross section of the SHG electric fields outside of the MM. These SHG field maps are generated from an infinite column of SRRs resonantly excited by a FF plane wave with the indicated polarization and direction. The electric- and magnetic-dipole-like patterns are clearly evident in the SHG radiation patterns.

These plots display a number of other prominent features. In particular, the contrasting symmetries in the nonlinear

properties of the two unit cells result in two distinct sets of nonlinear susceptibilities. The susceptibilities are highly dispersive, with different nonlinearities dominant at different frequencies. On the one hand, since the magnetic induction of the SRR must go to zero as the frequencies go to dc, we see that all of the nonlinearities vanish in this limit, with the exception of $\chi^{(2)}_{eee}$, which flattens out to a constant value nearly equal to the nonlinear dielectric alone. This nonresonant enhancement of the electric nonlinearity is impressive when considering that the nonlinear dielectric makes up less than 1 part in 50,000 of the MM's volume. On the other hand, when one of the involved frequencies is tuned near the magnetic-resonance frequency, we see that the overall nonlinear activity of the MM exceeds that of the nonlinear dielectric by orders of magnitude.

IV. EXAMPLES OF NONLINEAR MAGNETOELECTRIC PHENOMENA

Up until now, we have focused on the problem of constructing and characterizing nonlinear magnetoelectric MMs, but have avoided discussing how the full set of nonlinear susceptibilities can be used to achieve unique and interesting phenomena. Indeed, the parameter space that Eqs. (31)–(38) encompass is gigantic, especially when the tensorial nature of the nonlinear susceptibilities is considered. While it is beyond the scope of this paper to search out and categorize the range of phenomena that nonlinear magnetoelectric MMs can give rise to, this section is devoted to two demonstrative examples. First, we consider interference effects in MMs possessing two nonlinear susceptibilities of comparable magnitude. Having direct analogues in natural materials, nonlinear interference effectively tailors the harmonic and mix wave generation by suppressing and/or enhancing generation along certain directions, especially in optically thin slabs. Second, we analyze electro-optic effects in such MMs under the application of a static electric field. We show that, depending on geometry, the linear permittivity, permeability, and/or magnetoelectric coupling coefficient can be tuned by applying a voltage to the bulk MM. These examples are further illustrated through the prototypical SRRs of Sec. III B.

A. Nonlinear interference

From Fig. 3, it is clear that certain MM designs can support nonlinear processes with contributions from several effective nonlinear susceptibilities. The fields generated by the different nonlinearities can potentially interfere with each other, either enhancing or suppressing harmonic and mix wave generation. Nonlinear interference has been demonstrated in certain antiferromagnetic compounds [44–46], for example, in which $\chi^{(2)}_{eee}$ and $\chi^{(2)}_{mee}$ are found to have similar magnitudes. The process, however, is generally very weak and has been used mostly in probing the antiferromagnetic domains in such materials, using the fact that $\chi^{(2)}_{eee}$ reverses sign when going from one domain to another [64].

To offer a concrete example of nonlinear interference, let us consider collinear DFG in a homogeneous (or homogenized) medium, wherein forward propagating waves at ω_3 and ω_2 generate forward and backward waves at the frequency $\omega_1 = \omega_3 - \omega_2$. If we assume a sufficiently weak nonlinearity, we can take A_3 and A_2 to be constant, known as the nondepleted pump approximation. Assuming a slab of length L and no initial input at ω_1, Eq. (12) can be solved to give the intensities of the forward and backward DFG waves,

$$I_1(z) = \frac{1}{2} I_3 I_2 |\Gamma_{1,3,2^*}|^2 \mathrm{sinc}^2\left[(k_3 - k_2 - k_1)\frac{z}{2}\right] z^2, \quad (47)$$

$$I_{-1}(z) = \frac{1}{2} I_3 I_2 |\Gamma_{-1,3,2^*}|^2 \mathrm{sinc}^2\left[(k_3 - k_2 + k_1)\frac{L-z}{2}\right] (L-z)^2, \quad (48)$$

where, since we are considering DFG, the notation 2^* is used to indicate a negative frequency in calculating the coupling coefficient. Nonlinear interference, then, refers to the fact that the coupling coefficients in Eqs. (47) and (48) are superpositions of the eight second-order susceptibilities, which can add constructively or destructively in the generation of the forward and backward waves, $A_{\pm 1}$, depending on the relative phases and magnitudes of the susceptibilities, as well as the directionality of the involved waves. That is to say, $|\Gamma_{1,3,2}|$ is not necessarily equal to $|\Gamma_{-1,3,2}|$. Alternatively, if only one nonlinearity is dominant, then it is easy to verify that the magnitudes of the coupling coefficients are independent of inversion of any of the involved waves, or inversion of the medium itself.

While it may seem difficult and coincidental to find a MM supporting two second-order susceptibilities with similar enough magnitudes to make this effect noticeable, the permutation symmetries detailed above can lead to this behavior quite naturally. For example, let us consider DFG in the symmetric doubly-split ring resonator MM, or $\chi^{(2)}(\omega_1;\omega_3,-\omega_2)$ for $\omega_3 > \omega_{1,2}$. In particular, we take $\omega_3 a/2\pi c = 0.087$, close to the resonance frequency, while sweeping the other frequencies and calculate the associated nonlinearities, as shown in Fig. 4. Permutation symmetry implies that $\chi^{(2)}_{emm}(\omega_1;\omega_3,-\omega_2) \to \chi^{(2)}_{mme}(\omega_1;\omega_3,-\omega_2)$ in the limit $\omega_1 \approx \omega_2 \approx \omega_3/2$, resulting in the crossing point in Fig. 4(a). Since these are the dominant nonlinearities contributing to DFG, we see from Eq. (42) that $\Gamma_{1,3,2^*} \approx 2\gamma_{emm}$ and $\Gamma_{-1,3,2^*} \approx 0$ in the limit $\omega_1 \to \omega_2 \to \omega_3/2$, leading to unidirectional DFG in the forward direction.

For the same configuration, DFG in the antisymmetric SRR is dominated by both $\chi^{(2)}_{mmm}$ and $\chi^{(2)}_{eme}$, owing to a rough balance of the electric and magnetic coupling strengths at these frequencies, as shown in Fig. 4(b). However, these nonlinear susceptibilities are out of phase, in contrast to the previous example. The result is that *forward* DFG is suppressed, in favor of *backward* DFG. Such unidirectional behavior is fundamentally different from that associated with phase matching, and is in fact most noticeable in subwavelength slabs where phase-matching effects are negligible. Indeed, interference between nonlinear magnetoelectric susceptibilities offers an alternate route towards realizing unidirectional devices such as the nonlinear optical mirror [31]. The unidirectional behavior is further illustrated in the field maps shown in Figs. 4(c) and 4(d). Similar to Fig. 3, the field maps show a cross section of the DFG emanating from an infinite column of SRRs. The SRRs are excited by plane waves at the resonance frequency and half the resonance frequency, so that the DFG processes depicted in Figs. 4(c) and 4(d) correspond to the midpoints of Figs. 4(a) and 4(b), respectively, where the nonlinear interference is maximized.

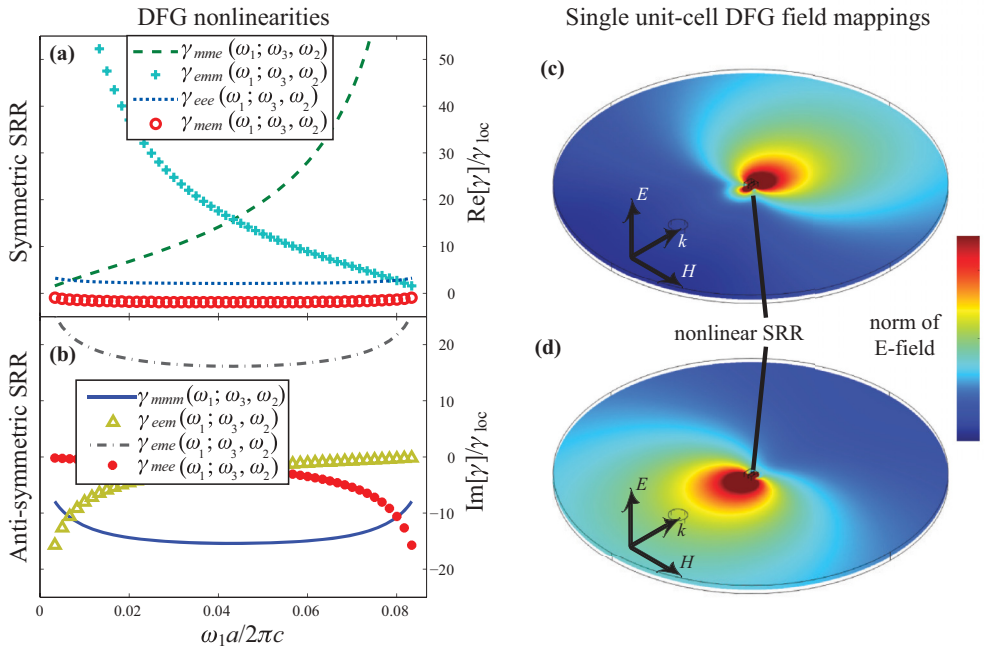

FIG. 4. (Color online) The second-order susceptibilities of the (a) symmetric and (b) antisymmetric SRRs for DFG, calculated via (31)–(38), for $\omega_3 a/2\pi c = 0.087$. (c) and (d) show field maps of DFG from infinite columns of symmetric and antisymmetric SRRs, respectively, in the nearly degenerate case. The comparable magnitudes in the two dominant nonlinear susceptibilities lead to unidirectional DFG, favoring forward generation in the symmetric SRR, and backward generation in the antisymmetric SRR.

B. Electro-optic effects

The tuning of optical properties is a highly desirable feature for many applications, and no less so in magnetoelectric media [41]. Since the metamaterials considered here have constituents that are susceptible to the electro-optic effect, it is natural to consider what effect a static electric field can have on all of the metamaterial's effective properties, as described by the effective second-order susceptibilities. Thus, let us consider the propagation of a monochromatic wave, labeled s, under the application of a static electric field, labeled 0. Under these conditions, we can show that the corresponding second-order susceptibilities are given by

$$\chi^{(2)}_{eee}(\omega_s;0,\omega_s) = \frac{1}{a^3}\iiint_{V_0} dV\left[\bar{\bar{\chi}}^{(2)}_{loc}(\vec{r}) : \vec{\theta}_0(\vec{r})\vec{\theta}_s(\vec{r})\cdot\vec{\theta}_s(\vec{r})\right], \tag{49}$$

$$\chi^{(2)}_{mem}(\omega_s;0,\omega_s) = \frac{1}{a^3}\iiint_{V_0} dV\left[\bar{\bar{\chi}}^{(2)}_{loc}(\vec{r}) : \vec{\theta}_0(\vec{r})\vec{\phi}_s(\vec{r})\cdot\vec{\phi}_s(\vec{r})\right], \tag{50}$$

$$\chi^{(2)}_{eem}(\omega_s;0,\omega_s) = \frac{i}{a^3}\iiint_{V_0} dV\left[\bar{\bar{\chi}}^{(2)}_{loc}(\vec{r}) : \vec{\theta}_0(\vec{r})\vec{\phi}_s(\vec{r})\cdot\vec{\theta}_s(\vec{r})\right], \tag{51}$$

$$\chi^{(2)}_{mee}(\omega_s;0,\omega_s) = -\frac{i}{a^3}\iiint_{V_0} dV\left[\bar{\bar{\chi}}^{(2)}_{loc}(\vec{r}) : \vec{\theta}_0(\vec{r})\vec{\theta}_s(\vec{r})\cdot\vec{\phi}_s(\vec{r})\right], \tag{52}$$

while all other nonlinearities must be identically zero. If we define the material relations according to

$$\vec{D}(\omega) = \bar{\bar{\epsilon}}\vec{E}(\omega) + i\bar{\bar{\kappa}}\vec{H}(\omega), \tag{53}$$

$$\vec{B}(\omega) = \bar{\bar{\mu}}\vec{H}(\omega) - i\bar{\bar{\kappa}}^*\vec{E}(\omega), \tag{54}$$

then it follows that the effective material properties are given by

$$\bar{\bar{\epsilon}}(\omega,\vec{E}_0) = \epsilon_0\left[1 + \bar{\bar{\chi}}^{(1)}_{ee}(\omega) + \frac{1}{\epsilon_0}\bar{\bar{\chi}}^{(2)}_{eee}(\omega;0,\omega) : \vec{E}_0\right], \tag{55}$$

$$\bar{\bar{\mu}}(\omega,\vec{E}_0) = \mu_0\left[1 + \bar{\bar{\chi}}^{(1)}_{mm}(\omega) + \frac{1}{\mu_0}\bar{\bar{\chi}}^{(2)}_{mem}(\omega;0,\omega) : \vec{E}_0\right], \tag{56}$$

$$\bar{\bar{\kappa}}(\omega,\vec{E}_0) = \frac{1}{c}\left[\bar{\bar{\chi}}^{(1)}_{em}(\omega) + \frac{c}{i}\bar{\bar{\chi}}^{(2)}_{eem}(\omega;0,\omega) : \vec{E}_0\right]. \tag{57}$$

In this context, it appears quite natural that $\chi^{(2)}_{eem}$ and $\chi^{(2)}_{mee}$ are purely imaginary for transparent media, such that the effective linear magnetoelectric coupling coefficients are real valued.

In essence, Eqs. (55)–(57) constitute the electro-optic effect for the linear electric, magnetic, and magnetoelectric properties, respectively. The corresponding second-order susceptibilities for the two MMs are shown in Fig. 5, approximating $\vec{\theta}_0(\vec{r})$ by a Bloch mode calculated at very low frequency. Thus, the symmetric SRR supports field-induced contributions to the permittivity and permeability. The antisymmetric SRR, on the other hand, supports field-induced magnetoelectric coupling. This is made particularly more interesting since magnetoelectric coupling in this SRR *vanishes* in the absence of an electric field. Similar control of optical activity has been realized in a chiral metamaterial through a third-order nonlinear process [65]. In this way, the linear magnetoelectric properties of a medium can be tuned dynamically.

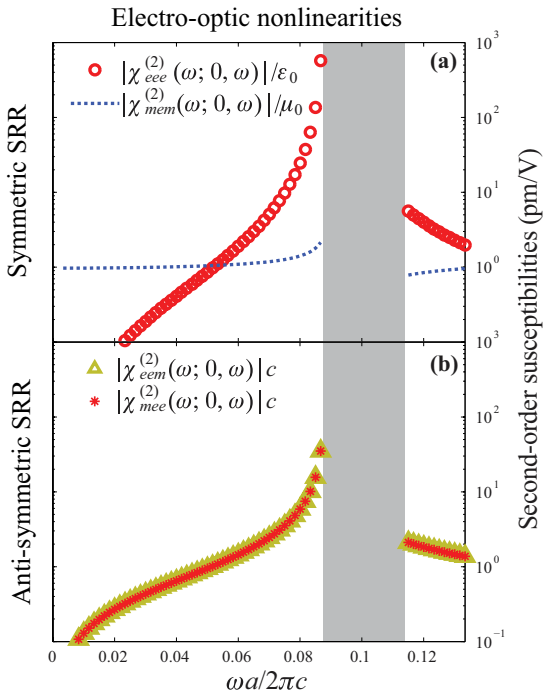

FIG. 5. (Color online) The effective second-order susceptibilities of the (b) symmetric and (c) antisymmetric SRRs under a static electric field, calculated via (49)–(52).

V. SPATIAL DISPERSION IN THE NONLINEAR SUSCEPTIBILITIES

As stated earlier, the expressions for the second-order nonlinearities in (31)–(38) are only valid in the limit $a \to 0$. In other words, they neglect the spatial dispersion effects in the material properties that accompany a finite unit-cell extent. In this section, we derive the leading-order effect of spatial dispersion in the nonlinear susceptibilities. In doing so, we find that the magnetoelectric nonlinearities naturally fall into two subsets depending on their tensorial nature (polar or axial), yielding two independent systems of equations. Using the simple case of a MM formed from a thin nonlinear slab periodically embedded in a dielectric matrix, we demonstrate that spatial dispersion tends to distribute a fundamental nonlinearity across the other three effective nonlinear susceptibilities of the same tensor type, analogous to spatial dispersion in the linear properties of MMs.

To obtain a more general set of expressions for the nonlinear susceptibilities that encompass spatial dispersion, homogenization can be achieved by direct comparison of Eq. (23) and the equivalent expression for a homogeneous material. Thus, casting the coupled-wave equations for a homogeneous medium, described by Eqs. (3) and (4), into the same integral form as Eq. (23) yields

$$\nabla A_\mu(\vec{R})\cdot\hat{s}_\mu = iA_\rho(\vec{R})A_\psi(\vec{R})\tilde{\Gamma}_{\mu,\rho,\psi}\frac{1}{a^3}\iiint_{V_0} e^{i(\vec{k}_\rho+\vec{k}_\psi-\vec{k}_\mu)\cdot\vec{R}}dV. \quad (58)$$

Applying the same restrictions to wave propagation and polarization as described in Sec. II C, we can equate the like terms in (58) and (23), implying that homogenization is achieved for

$$\begin{aligned}\frac{1}{a^3}\iiint_{V_0}&\left[\bar{\bar{\chi}}^{(2)}_{loc}(\vec{r}):\vec{e}_\rho(\vec{r})\vec{e}_\psi(\vec{r})\cdot\vec{e}^*_\nu(\vec{r})e^{i(k_\rho+k_\psi-k_\nu)z}\right]dV\\ &=\Big[\bar{\bar{\chi}}^{(2)}_{eee}\tilde{e}_\rho\tilde{e}_\psi\tilde{e}^*_\nu+\bar{\bar{\chi}}^{(2)}_{eme}\tilde{h}_\rho\tilde{e}_\psi\tilde{e}^*_\nu+\bar{\bar{\chi}}^{(2)}_{eem}\tilde{e}_\rho\tilde{h}_\psi\tilde{e}^*_\nu\\ &\quad+\bar{\bar{\chi}}^{(2)}_{emm}\tilde{h}_\rho\tilde{h}_\psi\tilde{e}^*_\nu+\bar{\bar{\chi}}^{(2)}_{mee}\tilde{e}_\rho\tilde{e}_\psi\tilde{h}^*_\nu+\bar{\bar{\chi}}^{(2)}_{mme}\tilde{h}_\rho\tilde{e}_\psi\tilde{h}^*_\nu\\ &\quad+\bar{\bar{\chi}}^{(2)}_{mem}\tilde{e}_\rho\tilde{h}_\psi\tilde{h}^*_\nu+\bar{\bar{\chi}}^{(2)}_{mmm}\tilde{h}_\rho\tilde{h}_\psi\tilde{h}^*_\nu\Big]\int_{-a/2}^{a/2}\frac{1}{a}e^{i(k_\rho+k_\psi-k_\nu)z}dz.\end{aligned} \quad (59)$$

This again represents eight equations containing eight effective second-order susceptibilities.

By comparing Eq. (59) with (29), we see that the approximation inherent in Sec. II C is equivalent to $\int_{-a/2}^{a/2}\frac{1}{a}e^{i(k_\rho+k_\psi-k_\nu)z'}dz'\approx 1$, i.e., the phase mismatch accumulated over a single unit cell is small. This is not always valid, as many MM unit cells have lattice constants that are not entirely negligible in comparison to the wavelength. As such, the previous steps cannot be repeated to yield a closed-form expression for each nonlinear susceptibility. For example, if we attempt to derive an expression analogous to (31), we find

$$\begin{aligned}\frac{1}{a^2}\iiint_{V_0}&\left[\bar{\bar{\chi}}^{(2)}_{loc}(\vec{r}):\vec{\theta}_1(\vec{r})\vec{\theta}_2(\vec{r})\cdot\vec{\theta}_3(\vec{r})\right]dV\\ &=\chi^{(2)}_{eee}\int_{-a/2}^{a/2}\cos(k_1z)\cos(k_2z)\cos(k_3z)dz+i\chi^{(2)}_{eme}\frac{\tilde{h}_1}{\tilde{e}_1}\int_{-a/2}^{a/2}\sin(k_1z)\cos(k_2z)\cos(k_3z)dz\\ &\quad+i\chi^{(2)}_{eem}\frac{\tilde{h}_2}{\tilde{e}_2}\int_{-a/2}^{a/2}\cos(k_1z)\sin(k_2z)\cos(k_3z)dz-\chi^{(2)}_{emm}\frac{\tilde{h}_1\tilde{h}_2}{\tilde{e}_1\tilde{e}_2}\int_{-a/2}^{a/2}\sin(k_1z)\sin(k_2z)\cos(k_3z)dz\\ &\quad-i\chi^{(2)}_{mee}\frac{\tilde{h}_3}{\tilde{e}_3}\int_{-a/2}^{a/2}\cos(k_1z)\cos(k_2z)\sin(k_3z)dz+\chi^{(2)}_{mme}\frac{\tilde{h}_1\tilde{h}_3}{\tilde{e}_1\tilde{e}_3}\int_{-a/2}^{a/2}\sin(k_1z)\cos(k_2z)\sin(k_3z)dz\\ &\quad+\chi^{(2)}_{mem}\frac{\tilde{h}_2\tilde{h}_3}{\tilde{e}_2\tilde{e}_3}\int_{-a/2}^{a/2}\cos(k_1z)\sin(k_2z)\sin(k_3z)dz+i\chi^{(2)}_{mmm}\frac{\tilde{h}_1\tilde{h}_2\tilde{h}_3}{\tilde{e}_1\tilde{e}_2\tilde{e}_3}\int_{-a/2}^{a/2}\sin(k_1z)\sin(k_2z)\sin(k_3z)dz.\end{aligned} \quad (60)$$

Rather than a single effective nonlinear susceptibility, the right-hand side appears to contain contributions from all eight. However, since the limits of the integrals on the right-hand side of Eq. (60) are symmetric, all of the terms containing odd integrands, or equivalently an odd number of sine terms, must vanish, leaving just four nonzero terms. This procedure can be repeated to find

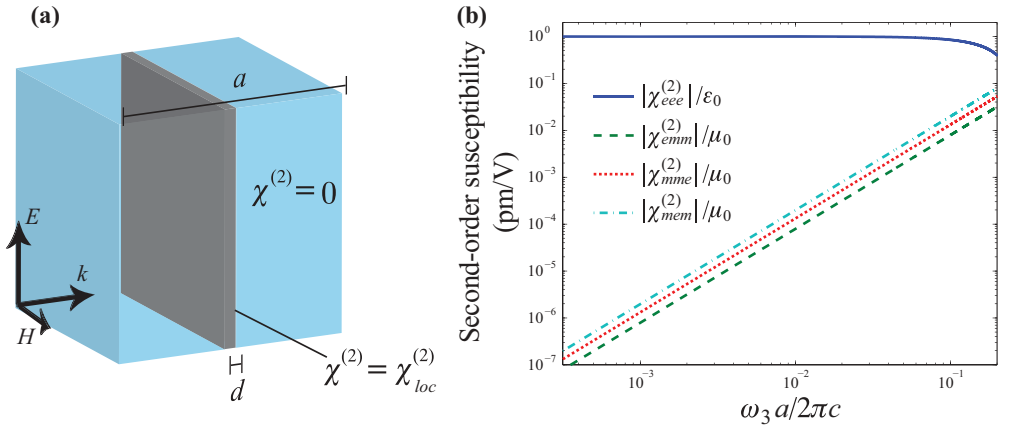

FIG. 6. (Color online) (a) Illustration of the unit cell for investigating spatial dispersion in the nonlinear properties, consisting of a thin nonlinear slab of thickness d embedded in a dielectric matrix with periodicity a. (b) The effective nonlinear susceptibilities, assuming $\epsilon_r = 2$, $d/a = 0.01$, $\chi^{(2)}_{loc}/\epsilon_0 = 100$ pm/V, $\omega_2 = 1.5\omega_1$, and $\omega_3 = \omega_1 + \omega_2$, as a function of $\omega_3 a/2\pi c$.

all eight analogous equations (see Appendix B). In doing so, the nonlinear susceptibilities naturally fall into two subsets, such that all of the terms from one subset or the other vanish in any given matrix element, leading to two independent systems of equations. The reason for this separation can be understood by considering the effective nonlinear tensor types. Specifically, for the construction considered here, the effective nonlinearities $\bar{\bar{\chi}}^{(2)}_{eee}$, $\bar{\bar{\chi}}^{(2)}_{mme}$, $\bar{\bar{\chi}}^{(2)}_{mem}$, and $\bar{\bar{\chi}}^{(2)}_{emm}$ are polar tensors, while $\bar{\bar{\chi}}^{(2)}_{mmm}$, $\bar{\bar{\chi}}^{(2)}_{eem}$, $\bar{\bar{\chi}}^{(2)}_{eme}$, and $\bar{\bar{\chi}}^{(2)}_{mee}$ are axial tensors. This follows naturally from the polar and axial vector nature of the electric and magnetic fields themselves, and the assumption that the local nonlinearity is a polar tensor [66]. Since spatial dispersion in this context should not depend on the handedness of the coordinate system, it follows that the affected susceptibilities must be of the same tensor type.

To see how a non-negligible unit-cell extent changes the effective nonlinear properties of a MM, let us use the example of a one-dimensional MM consisting of a thin nonlinear dielectric slab of extent d, periodically loaded in a dielectric spacer with period a, as shown in Fig. 6. For propagation normal to the slab, the field and polarization vectors become scalar. Moreover, to remove the effects of *linear* spatial dispersion, let us assume the slab and dielectric spacer have the same relative permittivity, ϵ_r. Thus, the Bloch modes are simple plane waves with $k_n = \sqrt{\epsilon_r}\omega_n/c$. In the long-wavelength limit, Eqs. (31)–(38) reveal that all of the effective nonlinear susceptibilities vanish except for the electric nonlinearity, which reduces to a simple volume average of the local nonlinearity,

$$\chi^{(2)}_{eee}(\omega_3;\omega_1,\omega_2) = \frac{d}{a}\chi^{(2)}_{loc} \quad \text{(long wavelength limit)}, \tag{61}$$

in agreement with previous studies of composite nonlinear media [61]. Since the nonlinear susceptibilities naturally separate into two subsets, the four axial nonlinear susceptibilities are identically zero for *all* wavelengths. This leaves us with a system of four equations and four unknown polar nonlinear susceptibilities. If $d = a$, i.e., the medium is simply a homogeneous slab of nonlinear dielectric, then (B1)–(B8) can be solved to give $\chi^{(2)}_{eee} = \chi^{(2)}_{loc}$ for all frequencies, as expected. On the other hand, in the limit $d \ll a$, the left-hand sides of (B2)–(B8) vanish. Solving this system to leading order in $k_i a$, we find

$$\chi^{(2)}_{eee} = \left[1 - \frac{1}{8}a^2\left(k_1^2 + k_2^2 + k_3^2\right)\right]\frac{d}{a}\chi^{(2)}_{loc}, \tag{62}$$

$$\chi^{(2)}_{emm} = +Z_1 Z_2\left(\frac{1}{12}a^2 k_1 k_2\right)\frac{d}{a}\chi^{(2)}_{loc} = +Z_0^2\left(\frac{\pi^2}{3}\frac{a^2}{\lambda_1\lambda_2}\right)\frac{d}{a}\chi^{(2)}_{loc}, \tag{63}$$

$$\chi^{(2)}_{mme} = -Z_1 Z_3\left(\frac{1}{12}a^2 k_1 k_3\right)\frac{d}{a}\chi^{(2)}_{loc} = -Z_0^2\left(\frac{\pi^2}{3}\frac{a^2}{\lambda_1\lambda_3}\right)\frac{d}{a}\chi^{(2)}_{loc}, \tag{64}$$

$$\chi^{(2)}_{mem} = -Z_2 Z_3\left(\frac{1}{12}a^2 k_2 k_3\right)\frac{d}{a}\chi^{(2)}_{loc} = -Z_0^2\left(\frac{\pi^2}{3}\frac{a^2}{\lambda_2\lambda_3}\right)\frac{d}{a}\chi^{(2)}_{loc}, \tag{65}$$

where $\lambda_n = 2\pi c/\omega_n$ is the wavelength in free space. Thus, spatial dispersion manifests itself in the susceptibilities of the same inversion symmetry, proportional to the square of the lattice constant-to-wavelength ratio. The second-order susceptibilities are plotted in Fig. 6(b) for typical values. While the above equations are specific to this example, the qualitative behavior and consequences of spatial dispersion in the nonlinear properties can be considered representative of MMs in general.

VI. CONCLUSION

Through a coupled-mode analysis, we have developed a method for describing the nonlinear behavior of MMs in terms of well-known nonlinear susceptibilities. These effective nonlinear susceptibilities are derived directly from the microscopic fields supported by the MM, giving a physically intuitive perspective of the nonlinear properties. By investigating these relations analytically and numerically, we have shown that the macroscopic nonlinear behavior of MMs can differ from its constituent materials not only in *magnitude* but in *kind*. In a simple dual-gap SRR medium, we were able to demonstrate a configuration and frequency combination at which each of the eight second-order susceptibilities, defined in Eqs. (3) and (4), was the dominant nonlinearity. However, it is likely that more interesting and beneficial structures can maximize the

usefulness of nonlinear magnetoelectric coupling, particularly chiral MMs, owing to the prominent role magnetoelectric coupling plays in such mediums.

To provide a context for this work, we note that certain magnetic materials are known to support wave-mixing processes, such as SHG, mediated through naturally occurring magnetoelectric nonlinearities [39–43]. These materials, however, are rare, and the strengths of such processes are limited by the weak optical magnetic responses of natural materials in general. In this context, the simple expressions in (31)–(38) show that MMs can potentially support similar processes, but at far higher efficiencies.

Perhaps most significantly, nonlinearities of different types can be brought together in a single medium in a controllable way that is simply impossible in naturally occurring materials. This implies a virtually boundless design space for the nonlinear properties of MMs. In particular, by combining nonlinear susceptibilities of roughly equal magnitudes in a single medium, one can access the phenomena of nonlinear interference, whereby the unidirectional generation of harmonics and mix frequencies can be achieved. Through clever design of the MM unit cell, nonlinear processes can be suppressed to avoid parasitic losses, or enhanced by orders of magnitude to form the core of compact, efficient nonlinear devices.

While we believe this work represents a fundamental step in understanding the nonlinear magnetoelectric properties of MMs, it is by no means intended to be an exhaustive description of the phenomena resulting from nonlinear magnetoelectric coupling. Indeed, inspired by the wide range of potential applications that have been found for various combinations of the linear electric, magnetic, and magnetoelectric properties of MMs, we hope that this work will spark similar creativity and ingenuity for combining the electric, magnetic, and magnetoelectric *nonlinear* properties of MMs in new and unforeseen ways, while laying the foundations for the design, characterization, and physics thereof.

ACKNOWLEDGMENTS

This work was supported by the Air Force Office of Scientific Research (Contract No. FA9550-09-1-0562). We thank Daniel Gauthier for helpful discussions.

APPENDIX A: COUPLED-MODE THEORY FROM MAXWELL'S EQUATIONS

In source-free media, Maxwell's macroscopic curl equations for the fields at frequency ω in the presence of a second-order polarization and magnetization are

$$\nabla \times \vec{E} = i\omega[\vec{B} + \mu_0 \vec{M}^{(2)}], \tag{A1}$$

$$\nabla \times \vec{H} = -i\omega[\vec{D} + \vec{P}^{(2)}], \tag{A2}$$

with the constitutive relations

$$\vec{D} = \bar{\bar{\epsilon}}\vec{E} + i\bar{\bar{\kappa}}\vec{H}, \tag{A3}$$

$$\vec{B} = \bar{\bar{\mu}}\vec{H} - i\bar{\bar{\kappa}}^*\vec{E}. \tag{A4}$$

Meanwhile, we know that, in the absence of the perturbation, the fields satisfy

$$\nabla \times \vec{\mathcal{E}}_\mu = i\omega\vec{\mathcal{B}}_\mu, \tag{A5}$$

$$\nabla \times \vec{\mathcal{H}}_\mu = -i\omega\vec{\mathcal{D}}_\mu, \tag{A6}$$

where we take $\vec{\mathcal{E}}_\mu$ and $\vec{\mathcal{H}}_\mu$ to represent the fields of some unperturbed mode μ with unitary amplitude. Assuming purely real material properties, we follow the path outlined in Ref. [59], combining Eqs. (A1)–(A6) to give

$$\begin{aligned}&\vec{\mathcal{H}}_\mu^* \cdot [\nabla \times \vec{E}] - \vec{E} \cdot [\nabla \times \vec{\mathcal{H}}_\mu]^* \\ &\quad = i\omega\vec{\mathcal{H}}_\mu^* \cdot [\vec{B} + \mu_0\vec{M}^{(2)}] - i\omega\vec{E} \cdot \vec{\mathcal{D}}_\mu^*\end{aligned} \tag{A7}$$

and

$$\begin{aligned}&\vec{H} \cdot [\nabla \times \vec{\mathcal{E}}_\mu]^* - \vec{\mathcal{E}}_\mu^* \cdot [\nabla \times \vec{H}] \\ &\quad = -i\omega\vec{H} \cdot \vec{\mathcal{B}}_\mu^* + i\omega\vec{\mathcal{E}}_\mu^* \cdot [\vec{D} + \vec{P}^{(2)}].\end{aligned} \tag{A8}$$

Adding Eqs. (A7) and (A8), we can apply some vector calculus identities to obtain

$$\nabla \cdot [\vec{E} \times \vec{\mathcal{H}}_\mu^* + \vec{\mathcal{E}}_\mu^* \times \vec{H}] = i\omega[\vec{P}^{(2)} \cdot \vec{\mathcal{E}}_\mu^* + \mu_0\vec{M}^{(2)} \cdot \vec{\mathcal{H}}_\mu^*]. \tag{A9}$$

From here, the coupled-mode equations can be found by choosing an explicit form for the fields $\vec{E}$ and $\vec{H}$ and the perturbations $\vec{P}^{(2)}$ and $\vec{M}^{(2)}$. In particular, by writing all field quantities in terms of an appropriate choice of basis modes for the unperturbed system, Eq. (A9) can be used to describe the evolution of a finite set of these modes in the presence of a sufficiently weak perturbation.

APPENDIX B: DERIVATION OF THE NONLINEAR SUSCEPTIBILITIES IN THE PRESENCE OF SPATIAL DISPERSION

Using the short-hand notation $S_n = \sin(k_n z)$ and $C_n = \cos(k_n z)$ and dropping the explicit integral limits, we can rearrange (29) into the following eight equations:

$$\begin{aligned}&\frac{1}{a^2}\iiint \left[\bar{\bar{\chi}}_{loc}^{(2)}(\vec{r}) : \vec{\theta}_1(\vec{r})\vec{\theta}_2(\vec{r}) \cdot \vec{\theta}_3(\vec{r})\right] dV \\ &\quad = \chi_{eee}^{(2)} \int C_1C_2C_3dz - \chi_{emm}^{(2)} \frac{\tilde{h}_1\tilde{h}_2}{\tilde{e}_1\tilde{e}_2} \int S_1S_2C_3dz + \chi_{mem}^{(2)} \frac{\tilde{h}_2\tilde{h}_3}{\tilde{e}_2\tilde{e}_3} \int C_1S_2S_3dz + \chi_{mme}^{(2)} \frac{\tilde{h}_1\tilde{h}_3}{\tilde{e}_1\tilde{e}_3} \int S_1C_2S_3dz,\end{aligned} \tag{B1}$$

$$\begin{aligned}&\frac{-1}{a^2}\iiint \left[\bar{\bar{\chi}}_{loc}^{(2)}(\vec{r}) : \vec{\phi}_1(\vec{r})\vec{\phi}_2(\vec{r}) \cdot \vec{\theta}_3(\vec{r})\right] dV \\ &\quad = -\chi_{eee}^{(2)} \frac{\tilde{e}_1\tilde{e}_2}{\tilde{h}_1\tilde{h}_2} \int S_1S_2C_3dz + \chi_{emm}^{(2)} \int C_1C_2C_3dz + \chi_{mem}^{(2)} \frac{\tilde{e}_1\tilde{h}_3}{\tilde{h}_1\tilde{e}_3} \int S_1C_2S_3dz + \chi_{mme}^{(2)} \frac{\tilde{e}_2\tilde{h}_3}{\tilde{h}_2\tilde{e}_3} \int C_1S_2S_3dz,\end{aligned} \tag{B2}$$

$$\frac{1}{a^2}\iiint\left[\bar{\bar{\chi}}^{(2)}_{loc}(\vec{r}):\vec{\theta}_1(\vec{r})\vec{\phi}_2(\vec{r})\cdot\vec{\phi}_3(\vec{r})\right]dV$$
$$=\chi^{(2)}_{eee}\frac{\tilde{e}_2\tilde{e}_3}{\tilde{h}_2\tilde{h}_3}\int C_1S_2S_3dz+\chi^{(2)}_{emm}\frac{\tilde{h}_1\tilde{e}_3}{\tilde{e}_1\tilde{h}_3}\int S_1C_2S_3dz+\chi^{(2)}_{mem}\int C_1C_2C_3dz-\chi^{(2)}_{mme}\frac{\tilde{h}_1\tilde{e}_2}{\tilde{e}_1\tilde{h}_2}\int S_1S_2C_3dz, \tag{B3}$$

$$\frac{1}{a^2}\iiint\left[\bar{\bar{\chi}}^{(2)}_{loc}(\vec{r}):\vec{\phi}_1(\vec{r})\vec{\theta}_2(\vec{r})\cdot\vec{\phi}_3(\vec{r})\right]dV$$
$$=\chi^{(2)}_{eee}\frac{\tilde{e}_1\tilde{e}_3}{\tilde{h}_1\tilde{h}_3}\int S_1C_2S_3dz+\chi^{(2)}_{emm}\frac{\tilde{h}_2\tilde{e}_3}{\tilde{e}_2\tilde{h}_3}\int C_1S_2S_3dz-\chi^{(2)}_{mem}\frac{\tilde{e}_1\tilde{h}_2}{\tilde{h}_1\tilde{e}_2}\int S_1S_2C_3dz+\chi^{(2)}_{mme}\int C_1C_2C_3dz, \tag{B4}$$

$$\frac{i}{a^2}\iiint\left[\bar{\bar{\chi}}^{(2)}_{loc}(\vec{r}):\vec{\phi}_1(\vec{r})\vec{\phi}_2(\vec{r})\cdot\vec{\phi}_3(\vec{r})\right]dV$$
$$=\chi^{(2)}_{mmm}\int C_1C_2C_3dz-\chi^{(2)}_{mee}\frac{\tilde{e}_1\tilde{e}_2}{\tilde{h}_1\tilde{h}_2}\int S_1S_2C_3dz+\chi^{(2)}_{eme}\frac{\tilde{e}_2\tilde{e}_3}{\tilde{h}_2\tilde{h}_3}\int C_1S_2S_3dz+\chi^{(2)}_{eem}\frac{\tilde{e}_1\tilde{e}_3}{\tilde{h}_1\tilde{h}_3}\int S_1C_2S_3dz, \tag{B5}$$

$$\frac{-i}{a^2}\iiint\left[\bar{\bar{\chi}}^{(2)}_{loc}(\vec{r}):\vec{\theta}_1(\vec{r})\vec{\theta}_2(\vec{r})\cdot\vec{\phi}_3(\vec{r})\right]dV$$
$$=-\chi^{(2)}_{mmm}\frac{\tilde{h}_1\tilde{h}_2}{\tilde{e}_1\tilde{e}_2}\int S_1S_2C_3dz+\chi^{(2)}_{mee}\int C_1C_2C_3dz+\chi^{(2)}_{eme}\frac{\tilde{h}_1\tilde{e}_3}{\tilde{e}_1\tilde{h}_3}\int S_1C_2S_3dz+\chi^{(2)}_{eem}\frac{\tilde{h}_2\tilde{e}_3}{\tilde{e}_2\tilde{h}_3}\int C_1S_2S_3dz, \tag{B6}$$

$$\frac{i}{a^2}\iiint\left[\bar{\bar{\chi}}^{(2)}_{loc}(\vec{r}):\vec{\phi}_1(\vec{r})\vec{\theta}_2(\vec{r})\cdot\vec{\theta}_3(\vec{r})\right]dV$$
$$=\chi^{(2)}_{mmm}\frac{\tilde{h}_2\tilde{h}_3}{\tilde{e}_2\tilde{e}_3}\int C_1S_2S_3dz+\chi^{(2)}_{mee}\frac{\tilde{e}_1\tilde{h}_3}{\tilde{h}_1\tilde{e}_3}\int S_1C_2S_3dz+\chi^{(2)}_{eme}\int C_1C_2C_3dz-\chi^{(2)}_{eem}\frac{\tilde{e}_1\tilde{h}_2}{\tilde{h}_1\tilde{e}_2}\int S_1S_2C_3dz, \tag{B7}$$

$$\frac{i}{a^2}\iiint\left[\bar{\bar{\chi}}^{(2)}_{loc}(\vec{r}):\vec{\theta}_1(\vec{r})\vec{\phi}_2(\vec{r})\cdot\vec{\theta}_3(\vec{r})\right]dV$$
$$=\chi^{(2)}_{mmm}\frac{\tilde{h}_1\tilde{h}_3}{\tilde{e}_1\tilde{e}_3}\int S_1C_2S_3dz+\chi^{(2)}_{mee}\frac{\tilde{e}_2\tilde{h}_3}{\tilde{h}_2\tilde{e}_3}\int C_1S_2S_3dz-\chi^{(2)}_{eme}\frac{\tilde{h}_1\tilde{e}_2}{\tilde{e}_1\tilde{h}_2}\int S_1S_2C_3dz+\chi^{(2)}_{eem}\int C_1C_2C_3dz. \tag{B8}$$

Equations (B1)–(B4) represent a system of four equations for the four polar second-order susceptibility tensors, while Eqs. (B5)–(B8) represent an independent system of four equations for the four axial second-order susceptibility tensors. Both systems can be solved using linear algebra.

[1] A. Lakhtakia, Electromagnetics **5**, 363 (2005).
[2] B. Wang, J. Zhou, T. Koschny, M. Kafesaki, and C. M. Soukoulis, J. Opt. A: Pure Appl. Opt. **11**, 114003 (2009).
[3] C. E. Kriegler, M. S. Rill, S. Linden, and M. Wegener, IEEE J. Quantum Electron. **16**, 367 (2010).
[4] J. B. Pendry, A. J. Holden, D. J. Robbins, and W. J. Stewart, IEEE Trans. Microwave Theory **47**, 2075 (1999).
[5] E. Shamonina, V. A. Kalinin, K. H. Ringhofer, and L. Solymar, J. Appl. Phys. **92**, 6252 (2002).
[6] E. Shamonina, Phys. Rev. B **85**, 155146 (2012).
[7] J. B. Pendry, D. Schurig, and D. R. Smith, Science **312**, 1780 (2006).
[8] E. Saenz, I. Semchenko, S. Khakhomov, K. Guven, R. Gonzalo, E. Ozbay, and S. Tretyakov, Electromagnetics **28**, 476 (2008).
[9] A. V. Rogacheva, V. A. Fedotov, A. S. Schwanecke, and N. I. Zheludev, Phys. Rev. Lett. **97**, 177401 (2006).
[10] E. Plum, V. A. Fedotov, A. S. Schwanecke, N. I. Zheludev, and Y. Chen, Appl. Phys. Lett. **90**, 223113 (2007).
[11] T. Kodera, D. L. Sounas, and C. Caloz, Appl. Phys. Lett. **99**, 031114 (2011).
[12] J. B. Pendry, Science **306**, 1353 (2004).
[13] M. Decker, M. W. Klein, M. Wegener, and S. Linden, Opt. Lett. **32**, 856 (2007).
[14] T. Q. Li, H. Liu, T. Li, S. M. Wang, F. M. Wang, R. X. Wu, P. Chen, S. N. Zhu, and X. Zhang, Appl. Phys. Lett. **92**, 131111 (2008).
[15] D.-H. Kwon, D. H. Werner, A. V. Kildishev, and V. M. Shalaev, Opt. Exp. **16**, 11822 (2008).
[16] B. Wang, T. Koschny, and C. M. Soukoulis, Phys. Rev. B **80**, 033108 (2009).
[17] Y. Ye and S. He, Appl. Phys. Lett. **96**, 203501 (2010).
[18] J. A. Reyes-Avendaño, U. Algredo-Badillo, P. Halevi, and F. Pérez-Rodríguez, New J. Phys. **13**, 073041 (2011).
[19] M. Ren, E. Plum, J. Xu, and N. I. Zheludev, Nature Commun. **3**, 833 (2012).
[20] R. A. Shelby, D. R. Smith, and S. Schultz, Science **292**, 77 (2001).

[21] D. Schurig, J. J. Mock, B. J. Justice, S. A. Cummer, J. B. Pendry, A. F. Starr, and D. R. Smith, Science **314**, 977 (2006).
[22] K. Guven, E. Saenz, R. Gonzalo, E. Ozbay, and S. Tretyakov, New J. Phys. **10**, 115037 (2008).
[23] A. A. Zharov, I. V. Shadrivov, and Y. S. Kivshar, Phys. Rev. Lett. **91**, 037401 (2003).
[24] M. W. Klein, C. Enkrich, M. Wegener, and S. Linden, Science **313**, 502 (2006).
[25] I. V. Shadrivov, A. A. Zharov, and Y. S. Kivshar, J. Opt. Soc. Am. B **23**, 529 (2006).
[26] M. A. Castellanos-Beltran, K. D. Irwin, G. C. Hilton, L. R. Vale, and K. W. Lehnert, Nature Phys. **4**, 929 (2008).
[27] E. Poutrina, D. Huang, and D. R. Smith, New J. Phys. **12**, 093010 (2010).
[28] V. M. Agranovich, Y. R. Shen, R. H. Baughman, and A. A. Zakhidov, Phys. Rev. B **69**, 165112 (2004).
[29] A. Popov and V. Shalaev, Appl. Phys. B **84**, 131 (2006).
[30] N. M. Litchinitser and V. M. Shalaev, Nature Photon. **3**, 75 (2009).
[31] A. Rose, D. Huang, and D. R. Smith, Phys. Rev. Lett. **107**, 063902 (2011).
[32] A. Rose and D. R. Smith, Opt. Mater. Express **1**, 1232 (2011).
[33] M. Scalora, M. S. Syrchin, N. Akozbek, E. Y. Poliakov, G. D'Aguanno, N. Mattiucci, M. J. Bloemer, and A. M. Zheltikov, Phys. Rev. Lett. **95**, 013902 (2005).
[34] I. Shadrivov, N. Zharova, A. Zharov, and Y. Kivshar, Opt. Express **13**, 1291 (2005).
[35] A. D. Boardman, P. Egan, L. Velasco, and N. King, J. Opt. A: Pure Appl. Opt. **7**, S57 (2005).
[36] A. Boardman, R. Mitchell-Thomas, N. King, and Y. Rapoport, Opt. Commun. **283**, 1585 (2010).
[37] R. W. Boyd, *Nonlinear Optics* (Academic, Burlington, MA, 2008).
[38] P. S. Pershan, Phys. Rev. **130**, 919 (1963).
[39] T. Rasing, J. Magn. Magn. Mater. **175**, 35 (1997).
[40] F. Jonsson and C. Flytzanis, Phys. Rev. Lett. **82**, 1426 (1999).
[41] M. Fiebig, J. Phys. D **38**, R123 (2005).
[42] F. Jonsson and C. Flytzanis, Phys. Rev. Lett. **96**, 063902 (2006).
[43] R. V. Pisarev, B. Kaminski, M. Lafrentz, V. V. Pavlov, D. R. Yakovlev, and M. Bayer, Phys. Status Solidi B **247**, 1498 (2010).
[44] M. Fiebig, D. Fröhlich, B. B. Krichevtsov, and R. V. Pisarev, Phys. Rev. Lett. **73**, 2127 (1994).
[45] Y. Tanabe, M. Fiebig, and E. Hanamura, in *Magneto-optics*, edited by S. Sugano and N. Kojima (Springer, New York, 2000).
[46] M. Fiebig, V. V. Pavlov, and R. V. Pisarev, J. Opt. Soc. Am. B **22**, 96 (2005).
[47] S. Larouche, A. Rose, E. Poutrina, D. Huang, and D. R. Smith, Appl. Phys. Lett. **97**, 011109 (2010).
[48] A. Rose, S. Larouche, D. Huang, E. Poutrina, and D. R. Smith, Phys. Rev. E **82**, 036608 (2010).
[49] A. Rose, D. Huang, and D. R. Smith, Appl. Phys. Lett. **101**, 051103 (2012).
[50] D. R. Smith, S. Schultz, P. Markoš, and C. M. Soukoulis, Phys. Rev. B **65**, 195104 (2002).
[51] D. R. Smith, D. C. Vier, T. Koschny, and C. M. Soukoulis, Phys. Rev. E **71**, 036617 (2005).
[52] D. R. Smith and J. B. Pendry, J. Opt. Soc. Am. B **23**, 391 (2006).
[53] C. Simovski, Opt. Spectrosc. **107**, 726 (2009).
[54] D. R. Smith, Phys. Rev. E **81**, 036605 (2010).
[55] A. Alù, Phys. Rev. B **83**, 081102 (2011).
[56] A. Alù, Phys. Rev. B **84**, 054305 (2011).
[57] H. Kogelnik, Bell Syst. Tech. J. **48**, 2909 (1969).
[58] A. Yariv, IEEE J. Quantum Electron. **9**, 919 (1973).
[59] J. Liu, *Photonic Devices* (Cambridge University Press, New York, 2004).
[60] J. D. Joannopoulos, S. G. Johnson, J. N. Winn, and R. D. Meade, *Photonic Crystals: Molding the Flow of Light*, 2nd ed. (Princeton University Press, Princeton, NJ, 2008).
[61] J. E. Sipe and R. W. Boyd, Phys. Rev. A **46**, 1614 (1992).
[62] S. Larouche and D. R. Smith, Opt. Commun. **283**, 1621 (2010).
[63] A. Rose, S. Larouche, and D. R. Smith, Phys. Rev. A **84**, 053805 (2011).
[64] R. V. D. Sa and C. Gros, Eur. Phys. J. B **14**, 301 (2000).
[65] I. V. Shadrivov, Appl. Phys. Lett. **101**, 041911 (2012).
[66] R. Birss, Rep. Prog. Phys. **26**, 307 (1963).